**Nationaal Lucht- en Ruimtevaartlaboratorium**
National Aerospace Laboratory NLR

NLR-TP-2000-421

# Vortex formation and flow separation: The Beauty and the Beast in aerodynamics

Lanchester 2000 Lecture

A. Elsenaar

**Nationaal Lucht- en Ruimtevaartlaboratorium**
National Aerospace Laboratory NLR

NLR-TP-2000-421

# Vortex formation and flow separation: The Beauty and the Beast in aerodynamics

Lanchester 2000 Lecture

A. Elsenaar

This report is based on a presentation held at the Royal Aeronautical Society, London, on May 4, 2000.



Division: Fluid Dynamics
Issued: August 2000
Classification of title: Unclassified

## Summary

Flow separation and vorticity generation are closely connected. When the flow leaves the trailing edge of a wing, a vorticity layer is formed, directly related to the lift of the wing and carrying streamwise vorticity. Boundary layers, in which the viscous flow very close to the wing surface is confined, carry vorticity in crosswise direction, perpendicular to the local flow direction at the boundary layer edge. Streamwise and crosswise vorticity are carried downstream in the wake.

When boundary layers separate from the surface ahead of the trailing edge, the flow characteristics are essentially similar though more complex. Vortex sheet separations of a more conical nature can be found on the upper surface of delta wing configurations or slender bodies of revolution. They can be regarded as a skeleton of vortex lines again with a strength related to lift and induced drag. These separations might be induced by sharp edges, as is the case for the sharp edged delta wing, or on smooth bodies, by boundary layer separation. Vortex sheet separations are not confined to conical geometries but can be found in all kinds of flow. Other separations on the wing will have a more bubble like nature, confined to a region close to the surface, and contributing to the viscous drag.

The distinction between streamwise and crosswise vorticity is preserved in the development of the wake downstream resulting finally, most often, in a pair of counter-rotating vortices that are of great concern from a safety point of view for landing aircraft. A simplified relation based on lift and induced drag can be used to estimate the strength of the vortices. They persist very long until the vortex pair breaks up trough a basic instability very far downstream.

A review is presented of these various types of separations and related vortex development, partly based on concepts as can be found in the literature. This is illustrated with practical examples of separations both from experiments and from CFD calculations.

## Contents



(58 pages in total)

## 1 Introduction

Ladies and gentlemen, it is an honor and a great pleasure to present this Lanchester Memorial Lecture. I thank the Royal Aeronautical Society and its Aerodynamic Committee for inviting me. In preparing this lecture I greatly enjoyed the added significance of presenting it in the historical context set by Lanchester. But the real pleasure is to be here among many good friends with whom I worked together for shorter or longer periods.

*"A body that in its motion through a fluid does not give rise to a surface of discontinuity"*. So defined Lanchester a '*streamline body'* in his standard work 'Aerodynamics' (1). With '*discontinuity'* the boundary is meant between the outer flow and the dead water region formed by fluid that *departs* from the surface as illustrated nicely in Fig. 1 for the flow around a cylinder.

What shape should a streamline body take? Fig. 2, also taken from 'Aerodynamics', is quite revealing. Lanchester shaped his streamline body around the inviscid flow pattern for a lifting ellipse. He realized that the ellipse would create in theory only, lift in this way: in practice the flow would depart from the surface: *'In all real fluids the influence of viscosity accounts for the departure, the departure being greater the less the viscosity* ' Lanchester noted. And he modified, inspired by the shape of a bird's wing, the ellipse with a long faired trailing edge '*to whittle away the abruptness of the ends*'.

This example reflects the theoretical knowledge at the time of Lanchester. As you can see in Table I, the publication of Lanchester's book *Aerodynamics* is right in the middle of the crucial theories that modeled the lift around a wing[1]. A real understanding of the trailing edge condition as formulated in the Kutta-Joukowsky theory, was not yet known. But these concepts 'were in the air' as illustrated by the fact that Lanchester himself contributed to the lifting line theory, for that reason referred to in this country as the Lanchester/Prandtl theory.

As illustrated in Fig.3 Lanchester made a distinction between a massive separation and a local separation bubble and he had a clear view of the formation of vorticity at the trailing edge of a lifting wing (Fig.4). So Lanchester was well aware of the fact that separations destroy the flow (hence my hint to a more beast like behavior), whereas the vortices are the cause of lift, required to realize our (beautiful) dream of flying.

I will try to put these concepts into an historical context, indicating and illustrating some of the major characteristics of separations and vortex formation. I selected this theme because I started my aerodynamic life at the National Aerospace Laboratory NLR in The Netherlands with an experiment on three-dimensional boundary separation, whereas at present I am trying to

[1] It should be noted that the original paper in which Lanchester describes the 'motion in periptery' (the fluid flow around a bird's wing) dates back to 1884/85. The paper was offered to the Physical Society of London, though rejected. Lanchester suggests that the referees were not familiar with the 'Newtonian method'.

understand the trailing vortices very far behind the aircraft. This and all that happens in between explains till today my fascination for aerodynamics.

## 2 The basics

### 2.1 The vortex sheet at the trailing edge

The *departure* of the flow from the trailing edge was not addressed explicitly in Lanchester's intuitive approach. The modelisation of the flow in this region by Kutta and Joukowski[2] and Prandtl[3] forms the starting point of this lecture. The flow over a *'streamlined'* wing leaves the trailing edge to form a vortex sheet that rolls-up further downstream as depicted by Lanchester in Fig.4. In the approximation as formulated in Prandtl's lifting line theory a system of straight vortex lines is assumed to leave the wing trailing edge, each with a strength defined by;

$$\gamma = \frac{\mathbf{d}\Gamma}{\mathbf{dy}}$$

with

$$\Gamma(\mathbf{y}) = \tfrac{1}{2}\mathbf{c}_{?}\mathbf{U}_{\infty}\mathbf{c}$$

the circulation for a wing section and depending on the local lift coefficient $\mathbf{c}_{?}$ and the local wing chord c, both functions of the spanwise coordinate y. The overall wing lift L follows from $\mathbf{L} = \rho\mathbf{U}_{\infty}\int_{-\mathbf{b}/2}^{\mathbf{b}/2}\Gamma(\mathbf{y})\mathbf{dy}$ with the wing span b, the free stream density $\rho$ and the free stream velocity $\mathbf{U}_{\infty}$. This system of vortices induces a flow angle at a particular wing station y that together with the geometrical angle of incidence provides the local circulation $\Gamma(\mathbf{y})$. The induced flow angle causes a rotation of the local lift force such that a force in free stream direction results that can be interpreted (approximately) as the induced drag:

$$\mathbf{D}_{\mathbf{ind}} = \frac{\mathbf{L}^2}{\tfrac{1}{2}\rho\mathbf{U}_{\infty}^2\mathbf{b}^2\pi.\mathbf{e}}.$$

The aerodynamic efficiency factor e can be derived from $\Gamma(\mathbf{y})$ and is equal to 1 for an elliptic distribution. Note that $\mathbf{D}_{\mathbf{ind}}$ is determined from inviscid theory only.

### 2.2 Laminar boundary layer separation

The crucial effect of viscosity as noted by Lanchester, could be modeled in a mathematical sense by the *boundary layer concept*, as formulated by Prandtl[4]: the effect of viscosity is only felt in a thin layer of fluid close to the body surface. The thickness of this thin layer ŭ is small

relative to the dimensions of the body L and typically of the order $\mathbf{L}/\sqrt{\mathbf{Re}}$ for the laminar boundary layer with the Reynolds number $\mathbf{Re} = \mathbf{U}_\infty \mathbf{L}\rho/\mu$ and ρ and μ the density and the dynamic viscosity respectively. Through the boundary layer the flow around the body exerts a frictional force on the body, the local wall shear stress $\tau_{wall}$ defined by:

$$\tau_{\mathbf{wall}} = \mu \frac{\mathbf{dU}}{\mathbf{dz}}\Big|_{\mathbf{z}=0}$$

U(z) is the velocity profile in the boundary layer in the direction z perpendicular to the surface. The boundary layer is responsible for the viscous drag $\mathbf{D}_{\mathbf{visc}}$, made up of the (over the surface of the body integrated) wall shear and the pressure drag (caused by the displacement of the inviscid flow due to the presence of the boundary layer). The wall shear stress is strongly influenced by the pressure distribution. In an adverse pressure gradient of sufficient strength $\tau_{wall}$ can become zero. The flow then leaves the surface and separation occurs.
Fig.5 provides an almost ideal view of a separation of a laminar boundary layer photographed by Van Ingen of Delft Technical University[5]. The point where the flow *departs* from the surface (in Lanchester's terminology) and the resulting discontinuity, are clearly visible. The separation point is a singular point in the boundary layer equations that describe this flow, the so-called Goldstein singularity[6]. However, the singularity can be removed by coupling locally the boundary layer development and the pressure gradient. We will meet this characteristic later again. Another important notion is the fact that the position of the laminar separation point depends on the (upstream history of the) pressure gradient and is (almost) independent of the Reynolds number. The only influence of the Reynolds number is due to the local displacement thickness that does change with Reynolds number and modifies the pressure gradient locally. As a result, the laminar separation will remain even in the limit of ReŸ Ð.

### 2.3 Turbulent boundary layer separation

The first project I was involved in at NLR was a theoretical and experimental study of a turbulent three-dimensional boundary layer on an infinite swept wing[7]. Berend van den Berg was the project leader and my tutor. In the experiment the infinite swept wing flow was simulated on a flat plate that formed one side of a skewed box. Fig.6b shows the surface streamlines on this flat plate made visible with oil. Fig.6a provides an interpretation of this flow. In this experimental set-up the pressure is constant in a direction parallel to the leading edge but increase in a direction perpendicular to it. The solid lines represent the external streamlines at the edge of the boundary layer. The dotted lines are the streamlines on the surface of the flat plate. From the difference in direction one can infer that inside the boundary layer the velocity vector rotates over an angle in excess of the angle over which the external flow is rotated. This stronger turning is caused by the fact that a streamline inside the boundary layer requires a

larger curvature due to its decreased velocity, to negotiate the pressure gradients. When moving further downstream this rotation increases till the wall streamlines run parallel to the leading edge or isobars (between station 8 and 9): a three-dimensional separation occurs. Wall streamlines that originate upstream can not pass this line. Beyond the separation line, the streamlines run almost parallel to the separation line.

This situation is quantified in Fig.7 that depicts the flow angles Ŭand (Ŭ+ƀ) at the edge of the boundary layer and the wall respectively when moving downstream. Separation occurs if the wall streamlines run parallel to the leading edge at about 55 degrees. Also the skin friction $C_f$ (the dimensionless wall shear stress) has been indicated. Note that the skin friction is far from zero at the separation point: it reaches a local minimum. Apparently, two different mechanism's have to be distinguished for three-dimensional separation: velocity reduction close to the surface due to the shear stresses and, as a consequence of that, a strong convergence of the streamlines close to the wall. For three-dimensional separations, the turning of the flow is the more important phenomenon.

The experiment was set-up as a validation experiment for a three-dimensional boundary layer method, using a turbulence model based on Peter Bradshaw's turbulent kinetic energy approach [(8)]. The results of the calculations with this method, presented as my first paper [(9)] for an AGARD conference in Göttingen in 1975, are shown in Fig.8a&b. The solid line represents the measured flow angle at the wall. The lower dotted line with the circles in Fig.8a is the calculation with the original turbulent model, a generalization of the existing two-dimensional turbulent kinetic energy method. In the experiment the turbulent shear stresses were measured indicating a shear stress that is clearly not in the direction of the local velocity gradient as the commonly used eddy viscosity models assume. When the turbulent model is modified according to these measured turbulent stresses the agreement greatly improves but only up to station 7. However, it appears that this result is very sensitive for the imposed pressure gradient: with a slightly increased pressure gradient separation is predicted but to early! Only when the pressure gradient is coupled to the local boundary layer displacement thickness (as illustrated in Fig.8b) a consistent result is obtained but only for the modified turbulence model. The example illustrates two things.

First, the singular behavior close to the separation point, similar to the Goldstein singularity for the laminar boundary layer. However, this singularity is not a property of separation itself, but of the boundary layer equations. The reason is the local interaction between the rapidly in thickness increasing boundary layer and the external pressure gradient. In those days computers were not big enough to solve the Reynolds averaged Navier Stokes equations and therefore the calculation was split-up in a viscous boundary layer part and an inviscid part. The coupling between these parts broke down at separation. Later the so-called 'strong interaction' provided a technique to handle this problem (see e.g. Le Balleur [(10)]). This problem is fully eliminated today by the ability to solve the Navier Stokes equations as one system and without the

necessity to use a boundary layer formulation. Secondly, the example shows that correct turbulence modeling is critical for the prediction of the separation position.

### 2.4 Conical separated flows

Separation so far has been discussed in the context of boundary layer theory. The laminar separation bubble as discussed before is a good example of a separation that is confined to the boundary layer. More examples of bubble like separations will be discussed later. In contrast to bubble like separations, separations with an open structure can also be observed in all kinds of flow. The classical example is the case of a sharp edged delta wing under incidence, for which the flow *departs* from the leading edge. This type of separation can be named after Maskell[11], *free vortex layer* or *vortex sheet separation.* The separation and the resulting formation of a vortex sheet that rolls-up into a vortex is basically inviscid. When the turbulent shear layer formed around the vortex sheet is neglected (true in the limit of infinite Reynolds number), the vortex sheet is bounded by inviscid flow on *both* sides. There the velocities are equal in magnitude but the directions are different. Consequently, the vortex sheet carries vorticity in the average flow direction, an essential feature of this separation. The vortex sheet that is formed at the leading edge of a delta wing is in principle similar to the vortex sheet that is formed at the trailing edge of a wing as described by the lifting line theory. In the latter case, however, the roll-up of the vortex layer takes place further downstream behind the wing. It is also not common to speak of separation fin the case of the trailing vortex sheet.
It is illustrative for the complexity of the flow that the modeling of the conical separated flow started 40 years after the formulation of the lifting line theory and covered a period of almost 30 years (see table II). The first model by Legendre[12] had a single vortex above the wing for which position and strength were adjusted such that the singularity at the wing leading edge was removed. The Royal Aircraft Establishment made subsequently very significant contributions in the development of an analytical model for this type of flow. The final solution of Smith[13] involved a precise formulation of the (removal of the) singularity at the leading edge, an approximation of the rolled-up vortex near its center and the introduction of a vortex sheet that connected the two[2]. In Prandtl's lifting line theory the vortices that leave the trailing edge could be approximated with a set of straight vortex lines in streamwise direction behind the wing. The roll-up process could be disregarded as a higher order effect. In the case of a conical delta wing the vortex is close to the wing surface and a precise representation of the sheet and the roll-up is essential.

[2] An excellent review with many references of this topic in a historical context by J.H.B. Smith can be found in ref.13.

### 2.5 'Smooth' separation

The location where the vortex sheet leaves the surface is geometrically determined by the sharp leading edge. In that case the flow could be handled as an inviscid problem. But when the leading edge radius is increased, (with a cone as a limiting case), the location where the vortex sheet is formed is far from obvious and three-dimensional boundary layer separation as discussed above, comes into the picture. J.H.B. Smith, F.T. Smith and Fiddes[14-18] have modeled this case analytically. The method of matched asymptotic expansions was used to account for the local interaction between the separating boundary layer and the pressure gradient. For a special condition named smooth separation, the curvature of the vortex sheet equals the curvature of the body. Smooth separation is found in the limit ReŸ Ð. It was further argued that the velocity downstream of the separation line (one might say the passive side) has to be tangential to the separation line, whereas the upstream velocity (on the active side) only has to be tangent to the body surface. These characteristics will be clearly visible in some of the pictures still to come. The concept of smooth separation implies that wall-streamlines on the body leave the surface and continue on the vortex sheet. It also follows from this theory that the separation can start very gradual, somewhere on the surface. The development of the theory has been greatly facilitated by the fact that laminar boundary layer separation is independent of the Reynolds number, as noted above. The analysis could hence be made for a fixed separation position and only the 'local' interaction had to be taken into account.
*Intuitively one is tempted to carry the concept of smooth separation over to the case of vortex sheet separation from a smooth surface with turbulent boundary layers.* To my knowledge such a generalization has not been pursued so far.

### 2.6 Separation and flow topology

In the publication by Maskell in 1955 on *Flow Separation in three dimensions*[11] and hence long before the theory for smooth separations was developed, a distinction is made between separations involving closed bubbles and separations involving free vortex layers or vortex sheets. This has been depicted schematically in Fig.9. Lighthill[19] formulated in 1963 a comprehensive approach in which the boundary layers and the trailing wake were described as thin layers of vorticity. The surface flow topology of skin friction or wall streamlines could be defined on the basis of different types of singular points. Wall streamlines can only leave the surface at singular points and in this context a line of separation was defined as *"a skin friction line that issues from both sides of a saddle point of separation and, after embracing the body disappears into a nodal point of separation"* [3].

[3] In the same article Lighthill mentions that 'some writers speak of skin friction lines as running into or having cusps on a line of separation (Maskell 1955)' and he continues with 'These statements have often very considerable approximate validity'.

The distinction between closed bubbles and open separations has started numerous studies and discussions following Lighthill's theory how separations should be defined and how they should be classified on the basis of surface streamlines [20-23]. Lighthill himself noted that separations from 'rounded' sharp leading edges comply with the general definition, although this required a '*degenerate node-saddle-node at the apex*'. It is also fair to state that within the framework of this theory it was a bit problematic to explain separations that started somewhere on the body surface (examples of which we will see later). *It is my tentative interpretation of the theory that the concept of smooth separation might provide a mechanism for wall streamlines to leave the surface along a line and not at singular points only, more in agreement with what is actually observed.*
A related question is if closed bubble separations can exist at all; see e.g. [23]. I will not go into more detail here but instead give some examples of observed separations.

## 3 Some examples of observed and calculated separations

### 3.1 Laminar separation bubbles

The first few examples will be related to bubble-like separations. The laminar separation bubble with turbulent reattachment slightly further downstream, is the most known example of a separation bubble. The laminar separation bubble typically occurs near the wing leading edge at higher incidences. The flow topology is similar to what has been indicated in Fig.9a. When reattachment occurs, the overall flow development is hardly effected. Locally, the pressure distribution is perturbed and the bubble will have some effect on the subsequent boundary layer development.

### 3.2 Shock wave boundary layer interaction

On transport type wings weak shocks are present at and around the design condition as illustrated in Fig.10. The symbols in Fig.10b show the pressure distribution as measured on a research wing of Aerospatiale half way the span. At 50% chord the shock is visible. The two lines in this graph are the results of Navier Stokes calculations made by Brandsma of NLR as part of a GARTEUR action group for this wing [24]. Results have been obtained with two different turbulence models. In Fig.10a the calculated wall streamlines are depicted. These calculations indicate a region underneath the shock that cannot be penetrated by the wall streamlines: a separation bubble is formed. The pressure distribution suggests also a separation underneath the shock. However, the effect of this local separation bubble on the pressure distribution is not well calculated. This should not come as a surprise: the very detailed complicated flow field of a shock-wave boundary layer interaction requires a degree of

refinement that is not yet present in the calculations. Note also that the trailing edge pressure, a measure for the *viscous* loading of the boundary layer, is not well predicted.
For fighters, massive separation due to (strong) shock wave boundary layer interaction is a very critical phenomenon that determines wing buffet, and hence the limits of flight. It can also give rise to unstationary phenomena like *'limit cycle oscillation'* (LCO). A nice example is shown in Fig.11, taken with a high speed camera in the transonic windtunnel HST of DNW for an oscillating straked delta wing at Mach= .9 near a condition of LCO[25]. In this smoke visualization, made during PIV measurements, three snapshots of the flow with increasing incidence are shown. In each picture the wing surface can be seen close to the bottom. In the first picture the shock is visible. This is also the case for the second picture, but now dark clouds come-in from the right side, what is believed to be a separated boundary layer. And finally, on the third picture the separated flow has killed the shock. This process repeats itself during each cycle of the limit cycle oscillation. The figure convincingly illustrates that a turbulent boundary layer separation for a condition of practical interest can be far away from the 'ideal' laminar separation as we have seen in Fig.5. Still, the separation seems to be confined to a region close to the wing surface.

### 3.3 Trailing edge separation

The boundary layer that passed successfully the leading edge peak and the shock wave must be able to withstand the pressure gradient over the rear of the airfoil close to the trailing edge. Fig.12 shows the oil flow pattern on a transport type wing just beyond the design condition as measured in the transonic tunnel HST of DNW as part of a GARTEUR study on the so called F4 wing, some 15 years ago [26]. The shock is clearly visible about midpoint of the chord. Outboard of the kink section along the trailing edge a region with separated flow is visible. The oil flow tests clearly indicated that oil flows from the lower to the upper surface. Just above and behind the trailing edge of the wing a thick viscous region is formed with some recirculating flow. This thick boundary layer is strongly coupled with the outer inviscid flow. Although the viscous layer will rapidly increase in thickness, the flow does not depart in a drastic way from the surface. This separation is again confined to a region close to the surface and therefore 'bubble-like'.
The combined effect of the shock wave boundary layer interaction and the subsequent downstream boundary layer development determines the condition at the trailing edge. And this in turn effects the overall circulation and hence the shock wave strength as indicated schematically in Fig.13 [27]. Since the shock wave boundary layer interaction and the wave drag, are very sensitive for shock strength, all the ingredients are present for a complicated Reynolds number sensitive viscous-inviscid interaction. This has been discussed extensively by Haines in the 27th Lanchester Lecture[28]. One remark should be made here. The flow variations resulting from this separation are generally gradual and continuous, up till the point that *'massive*

*separation'* occurs (involving a topological change in the overall flow field). If the shock is sufficiently weak, a little bit of separation at the trailing edge, causing some extra drag is not necessarily bad. This is somewhat similar to the situation at the optimal Lift/Drag ratio of a transonic wing where a weak shock is normally present and the resulting wave drag is accepted.

### 3.4 Leading edge separation on a delta wing

The previous examples showed more '*bubble like'* separations. The following examples are concerned with separations involving vortex sheets. The first two examples are taken from "The International Vortex Flow Experiment", a co-operation between FFA, DLR, AFWAL (Dayton OHIO) and NLR that started in 1983[29,30]. At that time the first result from CFD solutions for the Euler equations were obtained for the conical delta wing[4]. No explicit modeling of the vortex was required: it just came out of the solution! The elaborate analytical methods to describe this flow were superseded by new numerical techniques. Fig.14 shows the oil flow visualization in the nose region of the 65˚ delta wing (the configuration that was extensively studied) with a rounded leading edge at a Mach number of 85 and an incidence of 10 degrees. At that condition the flow is still attached close to the apex of the wing, though with a small laminar separation bubble. Further downstream, this separation bubble 'opens up' to form a separation with a free vortex sheet. An attachment line is formed more inboard with a separated flow region between this attachment line and the leading edge. This is an example of what can be called 'part span separation'. Due to the particular wing geometry the suction peak level is the strongest at the wing tip. As a result the separation starts at the wing tip and moves towards the apex with increasing incidence. It is an example where a bubble like separation changes gradually into an open, vortex sheet separation.

### 3.5 Secondary separation on a delta wing

The same delta wing, but now with a sharp leading edge, has been used extensively for the validation of Euler and Navier-Stokes codes. These calculations have been made by Brandsma of NLR[31]. The Euler code could calculate the separation and vortex formation that started from the leading edge but was of course unable to calculate the secondary separation underneath the vortex. This secondary separation is the result of the strong pressure gradient underneath the vortex. When Navier-Stokes codes became available in subsequent years they were able to catch this secondary separation. It is a nice example of a separation on a smooth surface as discussed above.

[4] The early Euler methods had problems with convergence when the Mach number was to low. For that reason already available low speed measurements could not be used to validate these new codes and an experiment was required at high subsonic Mach numbers.

### 3.6 Separation on an inclined cylinder

The next example (Fig.16) shows the flow over an inclined cylinder, an experiment performed at NLR in the seventies by Boersen[32]. The cylinder was covered with a thin foil that could be unwrapped to show more clearly the surface streamlines, as reproduced in Fig.16b. Here the windward attachment line is at the top. The flow is coming from the left. The white line clearly indicates separation. The surface streamlines hit this separation line at almost right angles. Behind the separation line the flow is more or less parallel to the separation line. This observation has resemblance to the reasoning of Smith for smooth body separations. At this particular Mach number the separation is shock induced, and this explains the very distinct features. This is in marked contrast with the very gradual way in which this separation starts. A GARTEUR Action Group, using an ONERA experiment as a test case, has recently calculated a very comparable flow (see Fig.17). The windward attachment line is here at the bottom of the figure. This case involves a primary but also secondary and even tertiary separation. The case shown has laminar boundary layer development. In that case a very good agreement is found between the measured (circles) and calculated (solid lines) primary separation positions. The figure shows the result of a calculation made by Prananta from NLR[33] but other contributors showed comparable results. It clearly proves the capabilities of today's CFD methods to describe complicated flows with vortex sheet separations on smooth surfaces. But a word of caution has to be made here as well. The corresponding turbulent case has also been calculated and this case indicated much larger differences with the experiment and between the various CFD methods. Variations up to 20 % have been reported for the calculated lift (all methods underpredicted the lift!). It is believed that deficiencies in turbulent modeling that fail to predict the correct location of the separation, are the cause of these discrepancies.

### 3.7 Separation involving a spiral vortex

The literature [e.g. 20-23] provides many examples of separations involving spiral points of separation. Fig. 18 is a particularly nice example. This particular flow pattern has been observed on the inner wing of the first 3-dimensional supercritical wing designed in The Netherlands in 1975 as part of a Fokker/NLR research program[34]. The separation is caused by a very strong spanwise pressure gradient in the wing root region[5]. The flow pattern is a good illustration of a separation that ends in a singularity as defined by Lighthill and involving in this case a spiral node. The vortex is similar to the one normally found at the trailing edge of the inboard wing when there is a strong decrease in inner wing loading. But in this particular case the vortex is

[5] The particular wing was designed by an (approximate) inverse method (quite advanced for that time!) under the inspiring leadership of Slooff. The 'target' pressure distribution was derived from quasi 2-D flow with additional reasoning at the wing root and tip. It appeared that the inverse problem was not well posed for the wing root. Strong geometrical constraints had to be applied to limit the range of possible shapes for a given 'target' pressure distribution. In discussing this lecture with Slooff, he indicated that the non-uniqueness of the solution for the inverse problem might be related to the fact that in the inverse problem the Kutta condition is nowhere stated explicitly: any separated flow condition (in the limit ReŸ Ð) is an allowable solution.

not formed near the trailing edge of the wing but more upstream on the wing itself. Of course, the formation of this vortex has a very strong effect on the inviscid flow in the sense that the topology of the flow field is changed fundamentally.

### 3.8 'Massive' separations

The regions with turbulent shear flow (or vortex layers in the sense of Lighthill) that are related to the separations discussed so far could still be considered as thin layers. They lie in the case of '*bubble like'* separations close to the surface and for *vortex sheet* separations close to the vortex sheet itself. But very often, like already illustrated in Fig.1 and 3, these regions are not thin at all. One can speak in that case of *massive separation.*

The space between the surface and the inviscid outer flow is then completely filled with (slow) circulating turbulent air. This will typically occur for bodies that are far away from a streamline shape or, for streamline shaped bodies, at very high incidences. Drag will be much higher and lift will be much smaller in comparison with streamline bodies. When lift is present, vortices in the wake (either steady or unsteady) will provide some structure to this flow.

### 3.9 A topological puzzle

This row of examples will be concluded with a topological puzzle: the flow over a delta wing of a supersonic transport configuration at high angle of attack. The configuration is the so called EUROSUP wing, a second generation supersonic transport wing designed and tested in the 4$^{th}$ Frame Work European Technology Program in a collaborative effort of Industry and Research Establishments [35]. Three design conditions were specified: *supersonic cruise*, *transonic cruise* and a *low speed climb-out* condition. The low speed design condition is characterized by the requirement that for the given planform a minimum drag has to be realized for a specific lift by optimizing a leading edge deflection. After the design, a windtunnel model was built and tested for the three design conditions in the Supersonic (SST) and Transonic (HST) tunnels of DNW. Fig.19 shows the low speed model mounted in the HST.

During the test the surface flow was visualized with oil (Fig.20). An analysis of this pattern is of interest as a further illustration of some of the separation types discussed above. The flow appears to have a number of streamwise vortices as visible in Fig.20a. The inner and outer part of the deflected leading edge is attached, whereas the middle part indicates a 'bubble like' separation. The oil flow in this region is reproduced somewhat enlarged in Fig.20b. A tentative interpretation of this flow is sketched in Fig.21. Two features are to be stressed. One is the development of a number of streamwise vortices, believed to be caused by vortex sheet separations as a result of the spanwise pressure gradients on this wing. Secondly, the separated flow on the middle part of the flap appears to have a more bubble like structure until it develops into a strong open separation further outboard. From the pressure distributions it can be seen

that this separation is the cause of a very strong vortex that moves rapidly outboard with increasing incidence. At higher incidence this vortex merges with a kind of conical tip vortex. This flow has also been calculated with Navier-Stokes codes as part of a follow-on study in GARTEUR. This study is still ongoing and only the calculated results of a first attempt by Jaap van Muyden of NLR[36] are reproduced here (Fig.22). These initial calculations have been made on a rather course grid of about 600.000 points provided by Hermann of DLR. Even on such a coarse grid some of the general features of this flow seem to be present. But when one looks into detail, there are very marked differences, notably in the prediction of the separated areas.

## 4 The beauty kisses the beast

I have tried to summarize in Fig.23 the various aspects of separation and vortex formation. The matrix is based on a distinction between separation from smooth surfaces and from sharp edges on the vertical axis and *'bubble like'* and *vortex sheet* formation on the horizontal axis. Examples of most of the named cases have already been presented. Contrary to what is claimed by some, I believe that 'bubble like' separations do occur in reality quite often. In this context I would like to quote Maskell[11] once more:
*"the fact that both these components* [bubbles and vortex sheet separations] *result from the same universal type of separation is particularly important, for it is then easy to understand how bubbles and free vortex layers exist together, and how one type of flow might develop gradually into another"*.
We have seen examples, like the part span vortex and the EUROSUP wing, where a 'bubble like' separation turns into an open vortex sheet formation. 'Bubble like' separation in three dimensions is very much a local affair. It can be viewed as a somewhat exceptional boundary layer development (see Fig.9a). As mentioned already, the velocity field in a boundary layer can be interpreted in the framework of a boundary layer concept (after Lighthill[19,37]) as a vorticity layer with cross-wise vorticity in a direction perpendicular to the local external inviscid velocity. For the three-dimensional boundary layer there is also a streamwise vorticity component, but this integrates to zero over the boundary layer since the crosswise velocity component is zero both at the boundary layer edge and at the surface: there is no mean streamwise vorticity. The same is true for the closed bubble. As in the case of the boundary layer, its effect in the downstream flow field is felt as a contribution to the total pressure losses. Vortex sheet separation (see Fig.9b) on the other hand has a pronounced effect on the overall flow topology, on the surface but even more so in the flow field away from the surface. A vortex sheet carries streamwise vorticity that is directly related to lift and induced drag.
For these reason I have added the captions *crosswise* and *streamwise vorticity* underneath the bubble and vortex sheet separation.

When does a ‘bubble like’ separation occurs and when vortex sheet formation? Under the shock wave for the transport type wing a bubble is found whereas the inclined cylinder shows the formation of a vortex layer. One is tempted to say that streamwise gradients favor more bubble like separations whereas crosswise velocity gradients can easily develop into vortex sheet separations. What actually happens depends on the proper match between the overall flow field and the local three-dimensional boundary layer development and separation. The EUROSUP example nicely illustrates this. For high aspect ratio wings the shed trailing vorticity is a function of the spanwise lift distribution. However, when the resulting spanwise gradients become too large, the boundary layer will separate ahead of the trailing edge and streamwise vorticity is shed through (a row of) vortex sheet separation(s). *If the vorticity cannot be turned in streamwise direction softly, it has to be done by brute (separation) force.*
It is very encouraging that the CFD methods of today seem to be able to make this match for rather complex flow topologies as some of the examples have indicated. Due to the fully implicit coupling with boundary layer growth, flows including separations can be calculated. But it is good to realize that, in the words of Maskell, a ‘*skeleton structure of vortex sheets*’ is hidden in the flow. And although boundary layers are no longer calculated explicitly in Navier Stokes solutions, the thin layer concept still stands on the surface and at the vortex sheet. An analysis of the flow along these lines, even when calculated by Navier-Stokes methods, provides valuable insight in the flow development. Also, a detailed and precise modeling of the three-dimensional separation is essential to predict the separation position correctly and hence to provide the correct lift and overall flow development. Turbulence modeling is critical here and the time has come that further progress is only possible with significant advances in this field. To understand *where in the flow* the turbulence modeling fails provides an additional argument for a ‘boundary layer type’ analysis.

# 5 ... and they had a long life together

## 5.1 The vortex field behind an aircraft

I have arrived at the epilogue. We have all looked in the sky and observed the white contrails of aircraft *en route* to their destination. You were looking at vortices. And you noticed that they can last for a long time. Wake vortices generated by landing aircraft do represent a safety problem as illustrated dramatically in Fig.24 for a *crop-spraying* plane. It is for this reason that strict *separation distances* have to be respected between landing aircraft varying from 4 to 6 nautical miles, depending on various combinations of aircraft weight. One might say that behind the aircraft the vortex is the beast and the separation the beauty. There is a safety issue but also an airport capacity issue: larger separation distances mean fewer landings in a given time. This explains the current explosion of activities in wake vortex studies.

As discussed, the flow field just behind an aircraft is composed of a vortex sheet carrying the vorticity that leaves the trailing edge and a number of discrete vortices from vortex sheet separations somewhere on the wing. This is typically the case for an aircraft in landing configuration. Large spanwise load variations are the cause of discrete vortices that originate at the wing tip, flap edges, the fuselage and tailplanes. This can be visualized in the windtunnel, using a rake with 5-hole probes to measure velocity magnitude and direction. Fig.25 shows the streamwise vorticity and the cross-flow velocity vectors as derived from the velocity measurements for various distances behind the model. Only one wing half is shown with the aircraft symmetry plane on the right side of each figure. Close behind the wing at a distance of 0.67 times the span, the vortex sheet is clearly visible with pockets of increased intensity, indicative of discrete vortices. The tip vortex can be clearly noted. Near the symmetry plane behind the fuselage exists a region with negative vorticity. When moving downstream the vortex sheet rolls-up and the various vortex cores merge into a simplified structure till at about 4.5 spans behind the aircraft two co-rotating vortices remain. These pictures were taken by Anton de Bruin, in the Low Speed Tunnel of DNW in a collaborative program with Boeing[38]. I will come back to this case later.

In the scheme of vortex formation and flow separation (Fig.23) a distinction was made between streamwise and cross wise vorticity. It can be shown that the streamwise vorticity relates to the induced rag $\mathbf{D}_{ind}$ through the crosswise velocity components **u** and **v** as follows:

$$\mathbf{D}_{ind} = \frac{1}{2}\rho\int(\mathbf{v}^2 + \mathbf{w}^2)\mathbf{dA} = \frac{1}{2}\rho\int \mathbf{v}_\vartheta^2\mathbf{dA}$$

The total pressure losses that originate in the boundary layers and at the shock waves relate to the crosswise vorticity and to the viscous and wave drag $\mathbf{D}_{visc}$ **+**$\mathbf{D}_{wave}$. Fig.26, similar to the previous one, visualizes these total pressure losses.

When comparing the two figures, one notes a clear correspondence in topology, but also large differences in intensity. The streamwise vorticity is most pronounced for the vortex that originates from the wing tip, whereas the total pressure losses, indicative of the viscous and pressure drag, cover a much wider area for the vortices that originated at the inner wing and fuselage. Not surprisingly: it reflects the characteristics of the lift and drag distributions over the aircraft components. The total pressure losses (related to the crosswise vorticity) are carried in a kind of passive way by the streamlines that derive their trajectories from the action of the streamwise vorticity.

The movement of the vortex sheet and imbedded vortices towards a situation with one (or possibly two) vortex pair(s) is called the roll-up process. This roll-up process can numerically be simulated. Starting from the velocity field as measured in the windtunnel just downstream of the aircraft, the subsequent development, including the merger of the different vortices, has been

visualized in Fig.27 by Laporte of CERFACS for an Airbus type aircraft in landing configuration. The vortices have been followed up to 20 spans downstream and in this particular case they seem to merge into a single vortex pair at that location.

### 5.2 Vortex strength

Behind the aircraft normally a single vortex pair develops. The distribution of the vertical velocity along a line that connects these vortices is shown in Fig.28a for an Airbus type aircraft in landing configuration as measured in the DNW by Hünecke with a 5-hole probe at about 7 spans behind the aircraft. Only one side of the symmetric distribution is shown. Three different regions in the vortex can be distinguished. Very close to the center of the vortex is the *viscous core* where the cross-wise velocity decreases rapidly towards the center of the vortex. The viscous core is embedded in a region where all vorticity in the flow is concentrated: the *vorticity core.* The distribution of the vorticity in this region is basically the result of the foregoing roll-up process. Viscosity is less important in this region. Further outboard finally the flow can be considered as basically inviscid and free of vorticity. In this *potential flow region* the velocity can be approximated by the superposition of two concentrated line vortices at the respective vortex centers. The strength of each of these vortices is given by:

$$\Gamma_0 = \frac{\mathbf{W}}{\rho \mathbf{U}_\infty \mathbf{bs}} = \frac{\mathbf{L}}{\rho \mathbf{U}_\infty \mathbf{bs}} = \tfrac{1}{2}\frac{\mathbf{C_L}.\mathbf{U}_\infty.\mathbf{b}}{\mathbf{AR}.\mathbf{s}}$$

and the velocity for each vortex follows from:

$$\mathbf{V}_\vartheta(\mathbf{r}) = \frac{\Gamma_0}{2\pi.\mathbf{r}}$$

Herein is $\mathbf{C_L}$ the lift coefficient of the wing with aspect ratio **AR**, the span **b** and the free stream velocity $\mathbf{U}_\infty$ . **s,** the distance between the vortex centers divided by the span **b,** is directly related to the spanwise lift distribution through:

$$\mathbf{s} = \int_{-1}^{1} \frac{\Gamma(\mathbf{y})}{\Gamma_0} \mathbf{d}(\mathbf{y} / \tfrac{1}{2}\mathbf{b})$$

with $\tilde{\mathbf{u}}_\mathbf{0}$ the circulation in the symmetry plane (**y**=0). **s** is, like the induced drag, determined by the spanwise lift distribution. For an elliptical distribution $\mathbf{s}=\frac{\pi}{4}$.

The velocity distribution in the *potential flow region* as composed of the individual contributions of the two line vortices is shown as the solid line in Fig.28a.

The velocity distribution in the *vorticity core* follows from the roll-up process but an *average* velocity in this region can be derived from the requirement that the integral of the cross flow velocities is related to the induced drag. Note that this level only depends on the spanwise load

distribution characterized by s, the aircraft geometry and lift, and the free stream velocity. This level has also been indicated in Fig.28a by the broken lines. Finally, the velocity in the core region is very difficult to measure and its quantification by calculation depends strongly on the applied turbulence model. For that reason, and also because of its small dimensions, this region has been neglected in the derivation of the average velocity in the *vorticity core*. Fig.28a suggests that this simple theory (named the 'flat vortex' approximation) is reasonably in accordance with the observed velocity distributions[6] and sufficiently representative for parametric studies.

Fig.28b shows a similar vortex characterization, but now behind another Airbus type aircraft during landing. The measurements have been made by Harris from DERA with a LIDAR system on Blagnac airport near Toulouse. As for the windtunnel measurements, the approximate velocity distribution (the 'flat vortex') derived from the wing geometry, aircraft speed and measured lift coefficient has been indicated. For the flight-tests the measured average velocity in the vorticity region is somewhat smaller than the predicted theoretical level, but this difference is probably related to the aging of the vortex (50 wing spans behind the aircraft) due to atmospheric turbulence that increases dissipation.

It should finally be remarked that the strength of the vortex and the velocity level inside the ('flat') vorticity core is a function of the dimensionless vortex spacing **s**. **s** can be influenced by the degree of inboard or outboard loading. This provides in principle a mechanism to reduce the severity of the vortex for a follower aircraft but the variations that can be realized are not very large.

### 5.3 Multiple vortices

The streamwise vorticity field does not necessarily rolls up into a single vortex pair since the interaction between different vortices is highly non-linear. In a NASA study by Bilanin et al [40] some possible flow topologies for a double vortex pair have been classified. This theoretical study dealt with two vortex pairs each with strength $\tilde{u}_1$ and $\tilde{u}_2$ and with positions $y_1$ and $y_2$ (see Fig.29). When the vortices are counter-rotating (negative $\tilde{u}_1/\tilde{u}_2$), and when the inner vortices are very close together and away from the outer ones ($y_1/y_2$ small), the inner vortices move rapidly away in upward direction. This situation might occur in the case of an aircraft with a heavy tailload. Something similar, but then with a movement in downward direction, can occur with a pair of two co-rotating vortices (the upper left part of the figure). For all other conditions the vortices seem to merge. However, Fig.25 suggest the possibility of a formation of a double pair of vortices. Such a condition can be met when the two vortices of each pair have about equal

[6] Surprisingly, the induced drag as an additional condition to quantify the velocity distribution in the vortex has been hardly used by others. Roberts (ref.46) uses this relation in his decay model with some success. Spreiter and Sacks (ref.44) have tried it with a Rankine vortex but reported 'unrealistically large cores'. In doing this they didn't make a distinction between the 'viscous core' and the 'vorticity core'. Moreover, neither a Rankine vortex nor a Lamb-Oseen vortex are of use here since they fix the ratio between the local velocity and the velocity given by the line vortex at the same radius (at a value of 1 respectively .714).

strength. The vortices then rotate around each other. The question mark in Fig.29 reflects the uncertainty with respect to the precise conditions for this to occur (added by the present author to the original analysis of Bilanin et al).

### 5.4 Vortex decay

Up till now vortex decay has not been taken into account. Spalart in his recent review in the Annual Review of Fluid Mechanics[41] states that there are two prevailing views: decay or collapse. For decay the strength of vortex gradually decreases in time. This is actually found in LIDAR measurements at e.g. the Heathrow and Blagnac airports[42]. The decay depends strongly on the turbulent conditions in the atmosphere. But will decay still occur in the absence of atmospheric turbulence? It has been observed that in a very quite atmosphere, the vortices last very long indeed (with Fig.28 as a typical example) where one would expect a gradual decrease due to dissipation and diffusion. This is apparently not the case. Many attempts have been made to explain and/or describe this behavior [43-47]. First of all it should be noted that the velocity distribution inside the *vorticity core* can be described by inviscid theory hence suggesting a minor role for viscosity. Moreover, the viscous core is usually (at the Reynolds numbers of interest here) very small. In a more recent publication Zeman[48] argues that due to damping effects of the strong curvature near the vortex center, the turbulent shear stresses can effectively be neglected. Hence only very small molecular diffusion is of importance at the viscous core only. With a plausible Reynolds stress model this could be quantified. All these arguments provide a possible explanation for the long life of vortices.

Are there other mechanism to destroy the vortex besides the significant effect of atmospheric turbulence and the very slow 'natural' decay? Crow[49] noticed a rapid decay after a long period with an almost constant vortex strength. One of these mechanisms[7] is related to a basic instability of the vortex pair and has been named after him *the Crow instability*. The two parallel vortex lines break-up into separate vortex rings. The occurrence of the Crow instability can be described by the non-dimensional time **Ű**defined by:

$$\tau = \frac{\mathbf{U}_\infty \mathbf{C}_\mathbf{L} \mathbf{t}}{4\pi \mathbf{ARbs}^3}$$

The Crow instability typically occurs in still air for values between 5 and 8[41]. This corresponds to separation distances of roughly the same order of magnitude or somewhat larger as actually prescribed in the regulations for separation distances. With atmospheric turbulence the critical value of **Ű**drastically decreases. It is of particular interest to note that for constant **Ű**, the time t

[7] Not all observed cases of rapid decay can be explained from the Crow instability; interesting enough the cause of other types of rapid decay is, to the author's knowledge, still very much an open question.

for the instability to develop is proportional to $\mathbf{s}^3$. Hence bringing the vortices closer together is a powerful mechanism to enhance instabilities.
Although the discussion of vortex instabilities is outside the scope of this lecture, it seems appropriate to conclude with a final example. It concerns the flow topology as presented in Fig.25 and discussed in relation with Fig.29. In that particular case the vortex sheet rolled up into two co-rotating vortices. Since the vortex system becomes more unstable when the distance between the vortices decreases, this flow topology favors the development of a more efficient instability mechanism. As a result the vortices break-up in a much smaller distance as normally required for the Crow instability. It is this mechanism that forms the basis of the recent Boeing patent in the names of Crouch and Spalart[50]. First a situation with a pair of two co-rotating vortices has to be achieved, by selecting an appropriate span loading. Next, the particular instability mode has to be activated through a well-defined periodic motion of the control surfaces (Fig.30). The combination of these causes a complete destruction of the vortices in a much shorter time, as illustrated in Fig.31 by large eddy simulation, also taken from the Boeing patent and probably the first Large Eddy Simulation to be reproduced in a patent.

*I have tried in my lecture to present you with a phenomenological view of separation and vortex formation. I have shown some examples of the complicated flow field on wings and slender bodies, a flow field that can be split into a field with streamwise and cross wise vorticity as clearly noticeable behind the wing. From there on this complex flow field simplifies, resulting in one or sometimes two vortex pairs. And this simplified flow field finally breaks up through vortex decay or instabilities into chaotic motion at smaller scales. And that is all that remains from the Tale of the Beauty and the Beast.*

**Acknowledgement**

Research should preferably be done in teamwork and across the border. I am very grateful that I could work in the international environment provided by GARTEUR, AGARD's Fluid Dynamics Panel and The International Vortex Flow Experiment. As part of the team the many colleagues both inside NLR and abroad should be mentioned that contributed to this lecture: Peter Bakker, Simon Boersen, Frans Brandsma, Anton de Bruin, Evert Geurts, Mike Harris, Sinus Hegen, Klaus and Caren Hünecke, Jan van Ingen, Florent Laporte, Jaap van Muijden, Bimo Prananta, Bernd Rohne and Joop Slooff.

Some colleagues have had a more profound influence on me and I would like to thank in particular 'my tutor in aerodynamics' and long time colleague Berend van den Berg. Equally Jaap van den Vooren for all discussions during the last year across the border between mathematics and my experimental/phenomenological/intuitive approach. And last but not least Frank Ogilvie for being such a stimulating boss.

Toulouse, spring 2000

## 6 References


| no | Author | title | source | year |
|---|---|---|---|---|
| 1 | Lanchester, F. W. | Aerodynamics, constituting the first volume of a complete work on aerial flight | London, Constable & Company Ltd, fourth edition of 1918 | 1907 |
| 2 | Joukowski, N.E. | Geometrische Untersuchungen über der Kutta'schen Strömung | Trans Physical Section of the Imperial Society of the Friends of Natural Science, Moscow | 1910/1912 |
| 3 | Prandtl, L. | Tragflügeltheorie, I & II | Mitteilungen nach der Königlichen Gesellschaft der Wissenschaft zu Göttingen | 1911/1919 |
| 4 | Prandtl, L. | Über Flüssigkeitsbewegung bei sehr kleiner Reibung | Verh.des III. Intern. Math. Kongresses, Heidelberg | 1904 |
| 5 | Ingen, J. van | Part of my forty years of teaching and research in boundary-layer flows: the laminar separation bubble | In: “Boundary layer separation in aircraft aerodynamics”, seminar dedicated to Prof. Jan van Ingen, Delft Technical University | 1997 |
| 6 | Goldstein, S. | On laminar boundary layer flow near a position of separation | Quart.J.Mech.Appl.Math 1, pp 43-69 | 1948 |
| 7 | Berg, B. van den, Elsenaar, A., Lindhout, J.P.F. and Wesseling, P. | Measurements in an incompressible three-dimensional turbulent boundary layer, under infinite swept wing conditions, and comparison with theory. | J.Fluid Mech, Vol. 70, part 1 | 1975 |
| 8 | Bradshaw, P, Ferris, D.H. and Atwell, N.P. | Calculation of boundary layer development using the turbulent energy equation | J.of Fluid Mech., Vol 28 pp 593-616 | 1967 |
| 9 | Elsenaar, A., Berg, B. van den and Lindhout, J.P.F. | Three dimensional separation of an incompressible turbulent boundary layer on an infinite swept wing. | AGARD CP-168; also NLR MP-75001U | 1975 |

| | | | | |
|---|---|---|---|---|
| 10 | Le Balleur, J.C. | Calcul par interaction visqueux non-viscueux des écoulements compressibles fortement décollés aux grandes portances sur profils d'ailes et voilures | AGARD CP-415 | 1992 |
| 11 | Maskel, E.C. | Flow separation in three dimensions | RAE Aero Rep. 2565 | 1955 |
| 12 | Legendre, R. | Écoulement au voisinage de la pointe avant d'une aile à flèche aux incidences moyennes. | 8th Int. Cong.Th.Appl.Mech., Istanbul | 1952 |
| 13 | Smith, J.H.B. | Vortical flows and their computation | RAE Tech.Memo AERO 1866 | 1980 |
| 14 | Smith, J.H.B. | Behaviour of a vortex sheet separating from a smooth surface. | RAE TR-77058 | 1977 |
| 15 | Smith, F.T. | Three-dimensional viscous and inviscid separation of a vortex sheet from a smooth non-slender body. | RAE TR-78095 | 1978 |
| 16 | Fiddes, S.P. | A theory of the separated flow past a slender elliptical cone at incidence. | AGARD CP-291 | 1980 |
| 17 | Fiddes, S.P. and Smith, J.H.B. | Calculations of axisymmetric separated flow past circular cones at large angle of incidence | AGARD CP-336 | 1982 |
| 18 | Fiddes, S.P. and Smith, J.H.B. | Asymptotic Separation from Slender Cones at Incidence | IUTAM Symposium 'Boundary layer separation', London, August 26-28, 1986 (Springer Verlag) | 1986 |
| 19 | Lighthill, M.J. | Introduction, Boundary Layer Theory | In: "Laminar Boundary layers", L. Rosenhead (ed.), Oxford University Press | 1963 |
| 20 | Peake, D.J. and Tobak, M. | Three-dimensional interactions and vortical flows with emphasis on high speeds | AGARDograph No. 252 | 1980 |
| 21 | Bakker, P.G. | A mathematical model for 'open' separation in three dimensional flow | In: "Essays on Aerodynamics", Delft University Press, pp 1-17 | 1992 |

| | | | | |
|---|---|---|---|---|
| 22 | Berg, B. van den | Physical aspects of separation in three-dimensional flows | In: “Boundary layer separation in aircraft aerodynamics”, seminar dedicated to Prof. Jan van Ingen, Delft Technical University | 1997 |
| 23 | Délery, J. | Topologie des écoulement tridimensionnels décollés stationnaires: point singuliers, séparatrices et structures tourbillonnaires. | ONERA, Rapport Technique No RT 121/7078 DAFE/N | 1999 |
| 24 | Brandsma, F. | ongoing work for GARTEUR AD(AG-26) | | 2000 |
| 25 | Geurts, E.G.M. and Cunningham jr, A.M. | Flow visualization and particle image velocimetry on a semi-span streaked delta wing, stationary and oscillating in pitch. | NLR TP-97261L | 1997 |
| 26 | Redeker, G. and Mueller, R., Ashill, P.R., Elsenaar, A. and Schmitt, V. | Experiments on the DFVLR-F4 wing body configuration in several european windtunnels. | in: AGARD CP-429 | 1987 |
| 27 | Elsenaar, A. | Observed Reynolds number effects on airfoils and high aspect ratio wings at transonic fow conditions. | in: AGARDograph 303; also NLR MP-88006U | 1988 |
| 28 | Haines, A.B. | "Scale Effect in Transonic Flow", the 27th Lanchester Memorial Lecture | Aeronautical Journal, August/September | 1987 |
| 29 | Elsenaar, A., Erikson, G. (ed) | Proceedings of the Symposium on the “International Vortex Flow Experiment on Euler Code validation”, Stockholm 1-3, 1986 | Published by FFA, Stockholm | 1986 |
| 30 | Elsenaar, A., Hjelmberg, L., Bütefisch, K., Bannink, W.J. | The International Vortex Flow Experiment | AGARD CP-437; also NLR MP-88019U | 1988 |
| 31 | Brandsma, F. | Private communication | | |

| | | | | |
|---|---|---|---|---|
| 32 | Boersen, S.J. | Reynolds number effects of pressure and normal force distributions along conically pointed circular cylinder at free-stream Mach number of 2.3. | NLR TR-75124U | 1975 |
| 33 | Prananta, B.B., Sytsma, H.A. and Amato, M. | Navier-Stokes calculations of supersonic flow about slender configurations – Results for an ogive cylinder configuration | GARTEUR TP-109-1 / NLR TR-99494 (Garteur Limited) | 1999 |
| 34 | Elsenaar, A. | Berekeningen van de drie-dimensionale grenslaag op de bovenzijde van de binnenvleugels van SKV-1 en SKV-2 | NLR TR-76124 (restricted) | 1976 |
| 35 | Lovell, D.A. | European research to reduce drag for supersonic transport aircraft | AIAA paper 99-3100 | 1999 |
| 36 | J. van Muijden | Private communication | | |
| 37 | Lighthill, M.J. | On Displacement Thickness | | 1958 |
| 38 | Bruin, A.C. de, Hegen, G.H., Rohne, P.B. and Spalart, Ph.R. | Flow Field Survey in Trailing Vortex System behind a Civil Aircraft Model at High Lift | AGARD Symposium “The characterisation and modification of wakes from lifting vehicles in fluids”, AGARD CP-584; also NLR TP-96284U | 1996 |
| 39 | Laporte, F. and Corjon, A. | Steady and unsteady 3D simulations of large civil aircraft wakes | European Congress on Computational Methods in Applied Sciences and Engineering, ECCOMAS 2000, Barcelona | 2000 |
| 40 | A.J. Bilanin, M.E. Teske, C.duP.Donaldson and R.S. Snedeker | Viscous effects in aircraft trailing vortices | In:”Wake Vortex Minimization”, NASA SP-409 | 1977 |
| 41 | Spalart, P.R. | Airplane Trailing Vortices | Annu.Rev.Fluid Mech. , No. 30, pp 107-138 | 1998 |
| 42 | Harris, M. | Private communication | | |
| 43 | Squire, H.B. | The growth of a vortex in turbulent flow | Aeronautical Quarterly, Vol.16 | 1965 |

| | | | | |
|---|---|---|---|---|
| 44 | Iverness, D.J. | Correlation of turbulent trailing vortex decay data | J.Aircraft Vol 13, No 5 | 1976 |
| 45 | Spreiter, J. R., Sacks, A.H. | The rolling up of the trailing vortex sheet and its effect on the downwash behind wings | Journal of Aeronautical Sciences, Vol. 18 | 1951 |
| 46 | Roberts, L. | Persistence and decay of wake vorticity | AGARD CP-187 | 1975 |
| 47 | Ciffone, D.L. and Orloff, K.L. | Far-Field Wake-Vortex Characteristics of Wings | J.Aircraft Vol 12, No 5 | 1975 |
| 49 | Crow, S.C. | Stability theory for a pair of trailing vortices | AIAA J.Vol 8, No 12, pp 2172-2179 | 1970 |
| 50 | Crouch, J.D. and Spalart, P.R. | Active system for early destruction of trailing vortices | Patent with International Publication Number: WO 99/00297 | |

Table I.

## AERODYNAMIC THEORIES AT THE TIME OF LANCHESTER

- 1904: boundary layer concept by Prandtl
- 1905: LIFT=ρ.U.Γ after Joukowski
- 1907: publication of ‘Aerodynamics’ by Lanchester
- 1910: formulation of Kutta-Joukowski condition
- 1911: lifting line theory by Prandtl

Table II

## ANALYTICAL MODELS FOR THE SEPARATION ON DELTA WINGS

- 1952: Line vortex model of Legendre
- 1954: Brown and Michael added a vortex sheet from LE to vortex core
- 1959-1968: conical vortex sheet model by Mangler and Smith (including ‘Kutta condition’ and vortex sheet ‘roll-up’)
- 1977-1980: Smith, Smith and Fiddes: separation from smooth surfaces

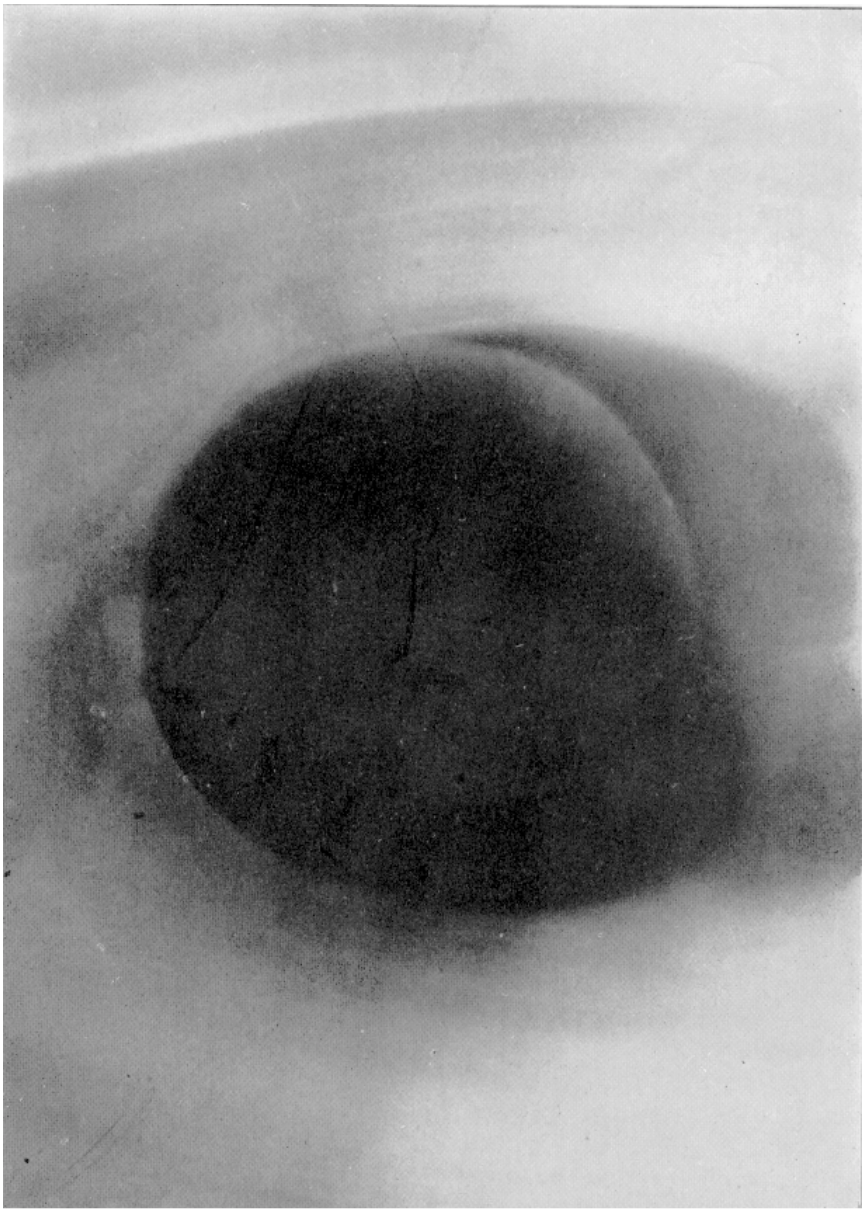


*Figure 1. "Photograph Showing Flow of Air Round a Cylinder in Motion" as taken by Lanchester.*

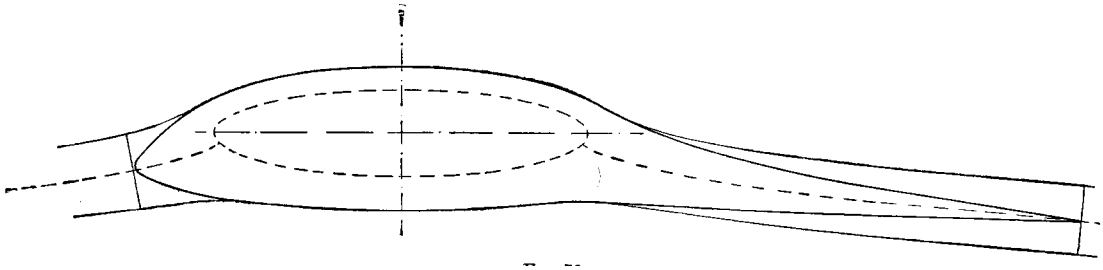

*Figure 2. The shape of a streamline body as sketched by Lanchester.*

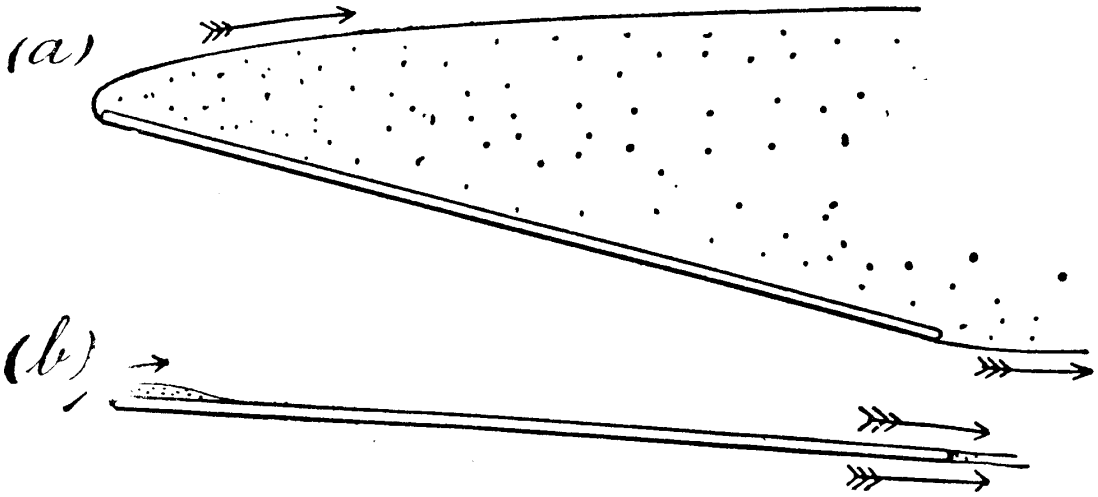


*Figure 3. Sketch by Lanchester of a massive separated flow (a) and a local separation bubble (b) for a flat plate.*

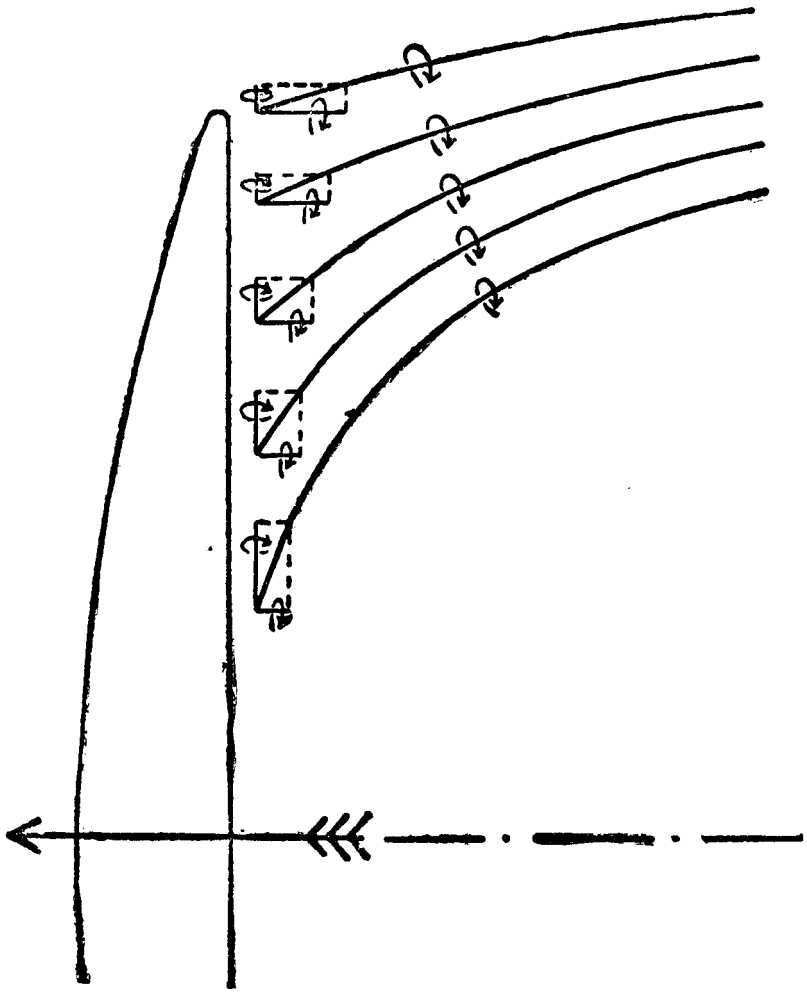

*Figure 4. The trailing vortex system for a lifting wing viewed by Lanchester.*

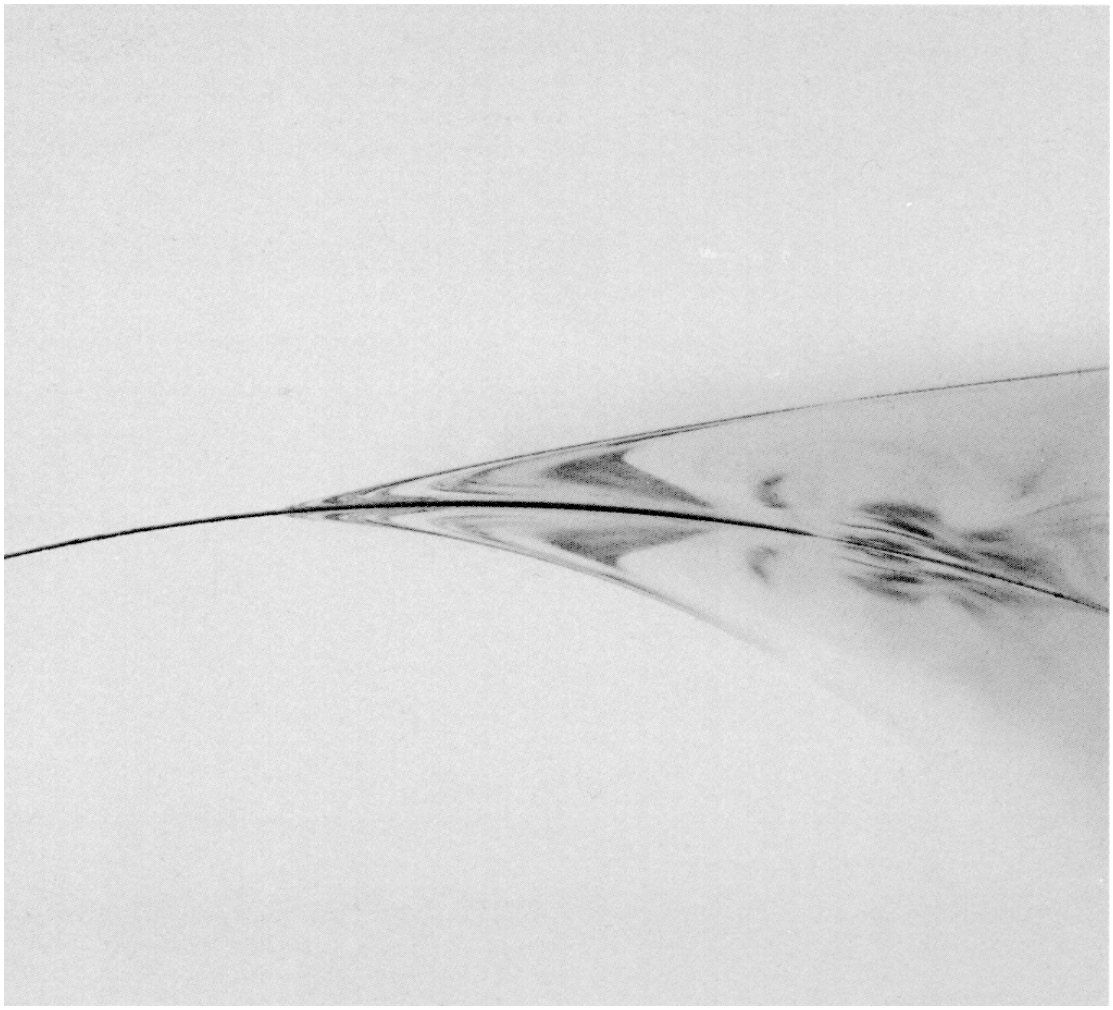

*Figure 5. Separation of a laminar boundary layer by Van Ingen of Delft Technical University.*

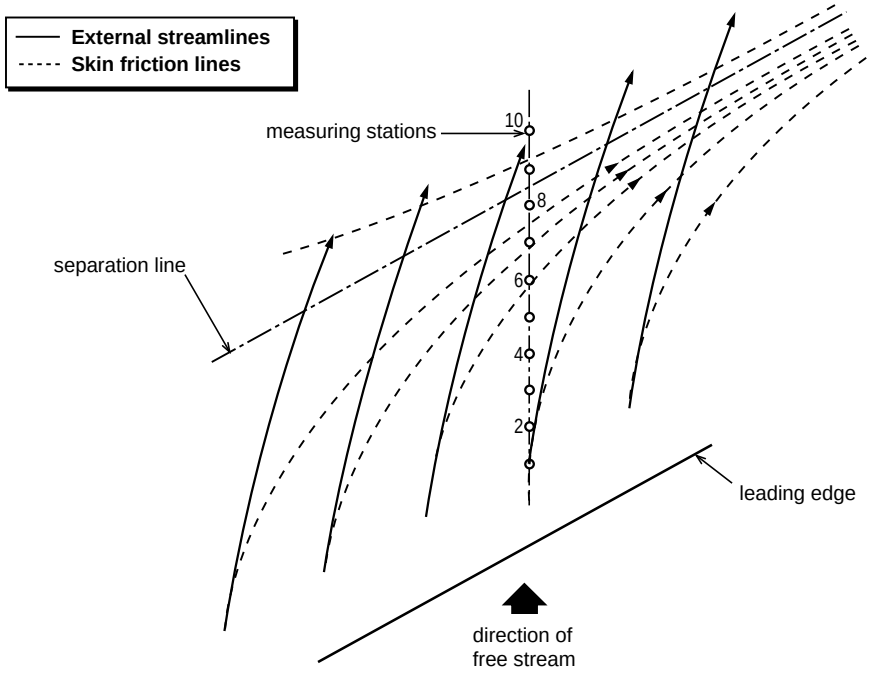


*Figure 6a. Interpretation of the flow simulating an infinite swept wing; the external streamlines and the wall streamlines have been indicated in relation with the separation line (NLR research program)*

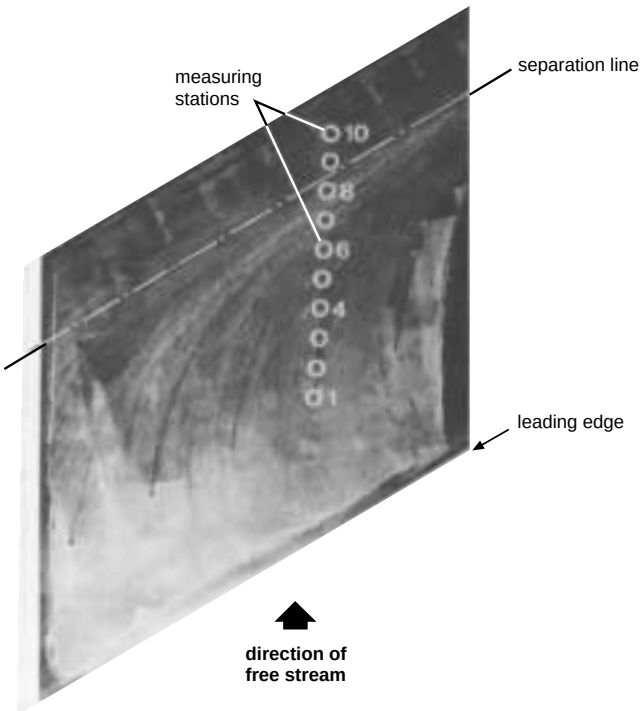


*Figure 6b. Oil flow pattern of the flow simulating an infinite swept wing.*

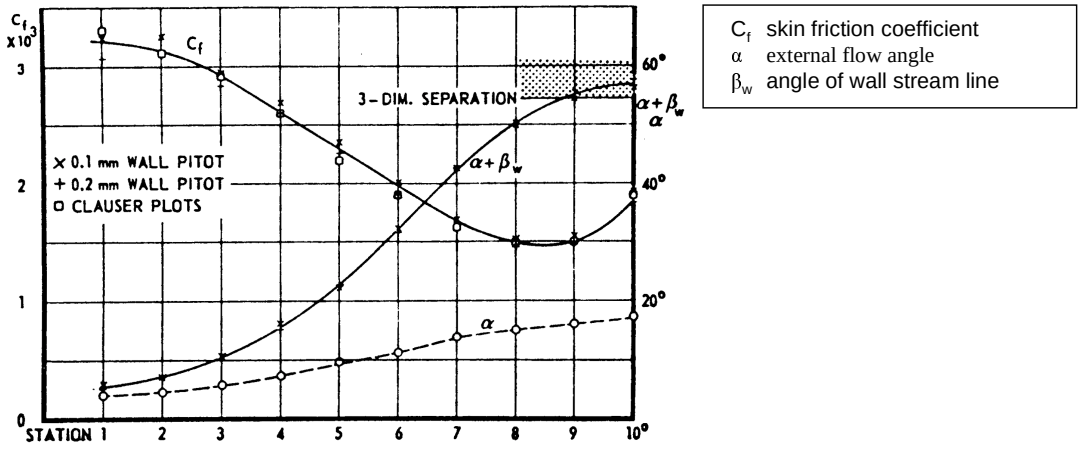


*Figure 7. Flow angles at the edge of the boundary layer (α) and at the wall (α+β) for the infinite swept wing experiment; separation occurs when the wall streamlines run parallel to the leading edge of the flat plate; the skin friction reaches at that location a minimum.*

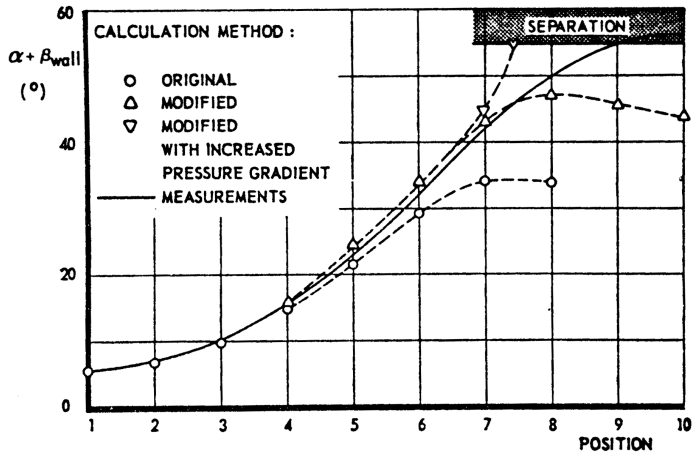


a) calculation with prescribed pressure distribution

*Figure 8a. Results of boundary layer calculations for the infinite swept wing case with a prescribed pressure distribution; note improvement by modifying the turbulence model according to the measured turbulent stress tensor; an overshoot occurs when the pressure gradient is slightly increased.*

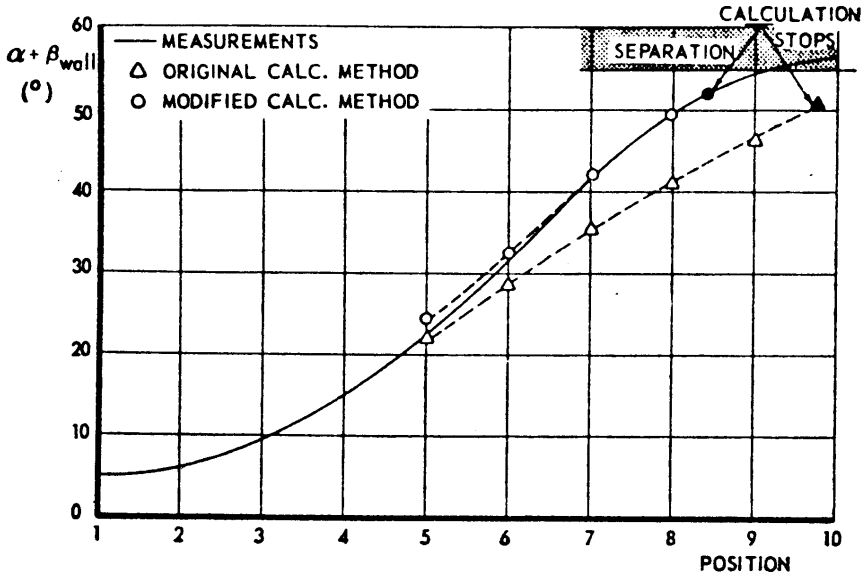


b) calculation allowing for interaction

*Figure 8b. Results of boundary layer calculations for which the pressure gradient is determined in interaction with the calculated boundary layer displacement thickness; good agreement is obtained when the turbulence model is modified according to the measured turbulent stress tensor.*

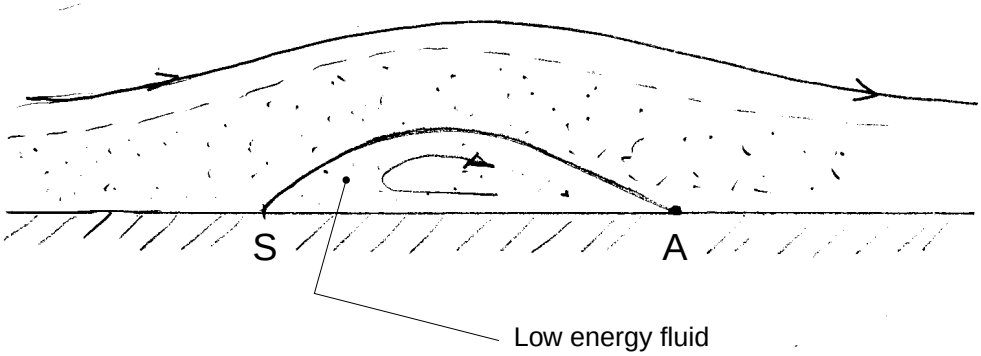


*bubble (2D-cut)*

*Figure 9a. Schematic view of a 'bubble like' separation confined to the boundary layer.*

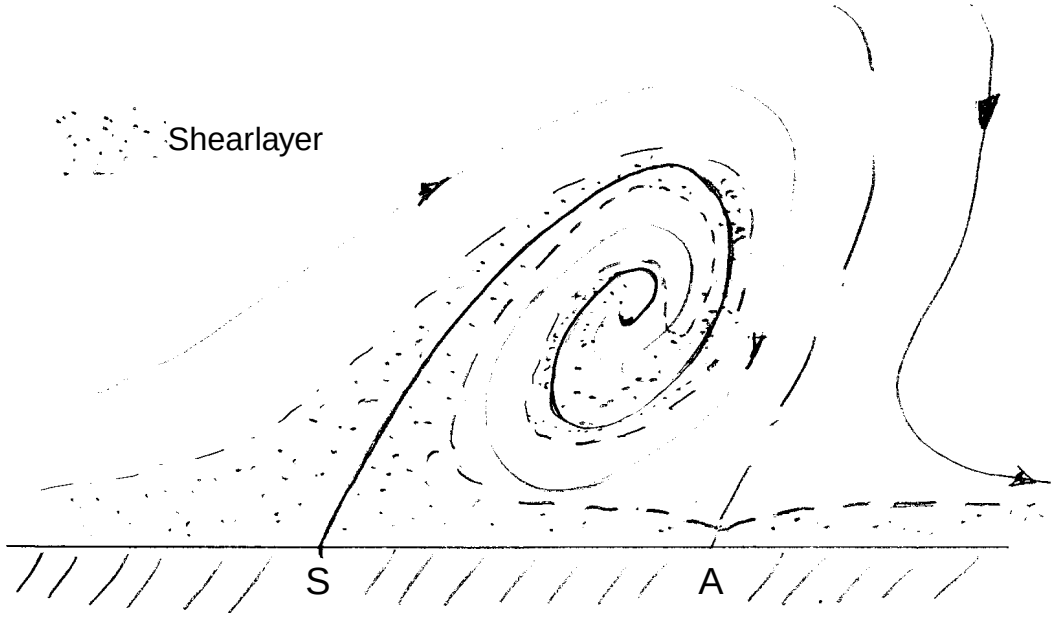


*open separation (2D-cut)*

*Figure 9b. Schematic view of an 'open' separation: a vortex sheet leaves the surface and rolls-up into a vortex.*

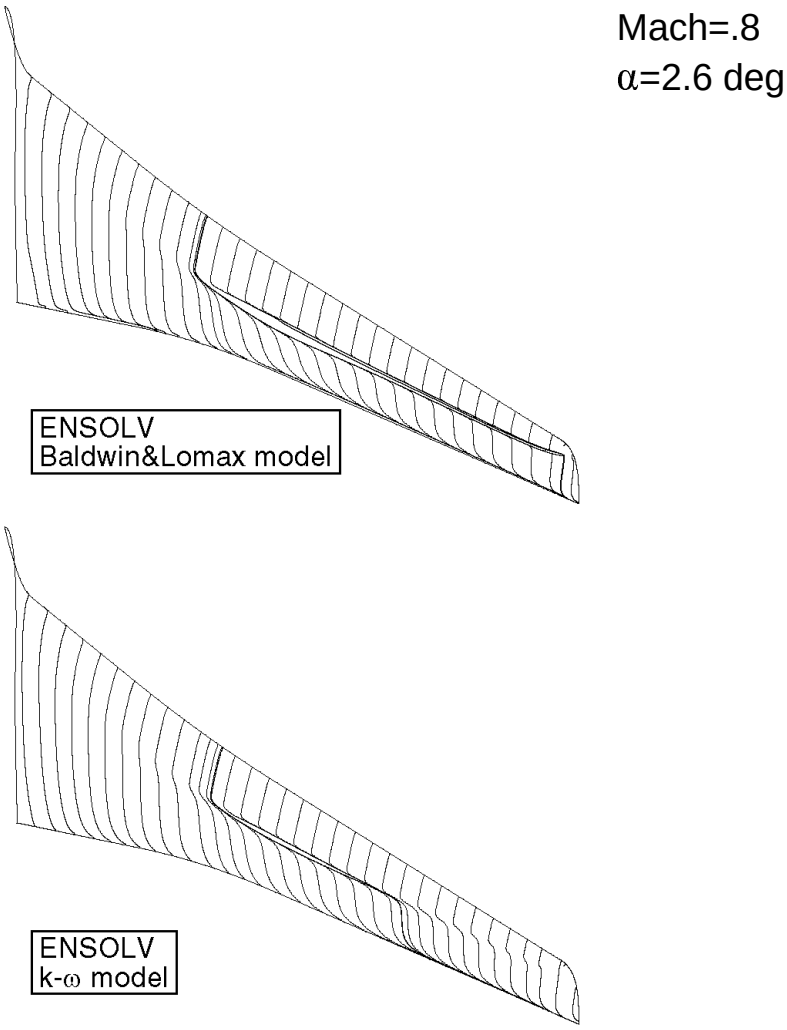


*Figure 10a. Navier-Stokes calculations of wall streamlines with two turbulent models for a representative transport type wing; under the shock a local separation bubble is visible (Aerospatiale wing; NLR/GARTEUR calculations).*

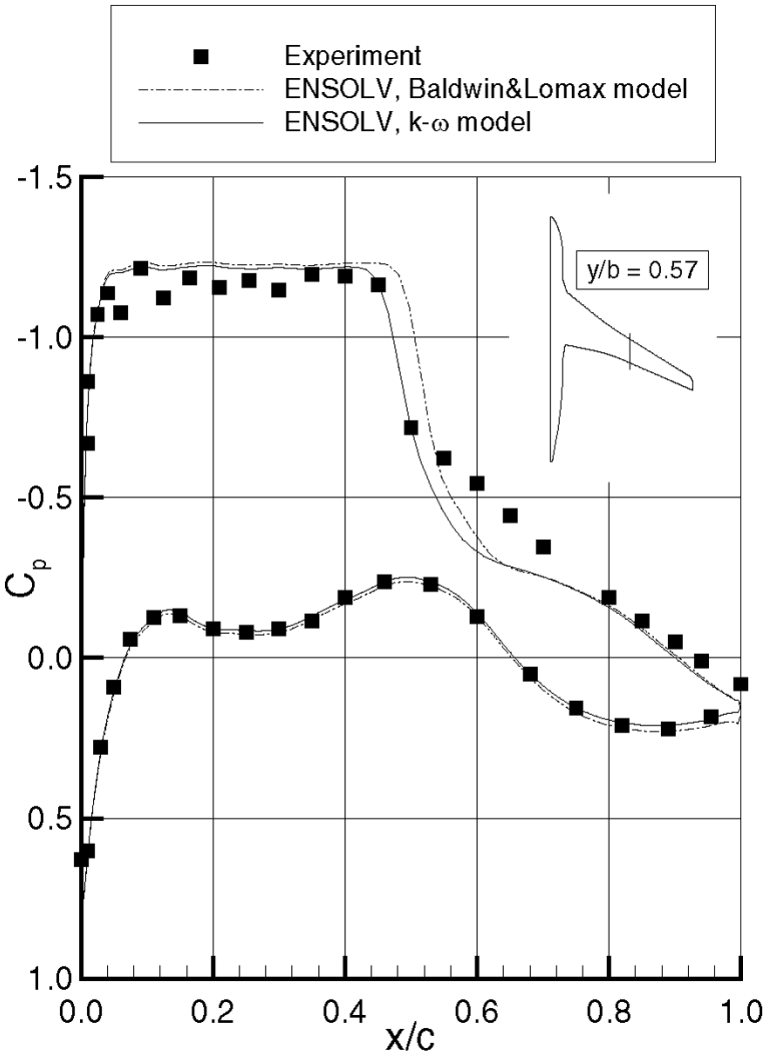


*Figure 10b. Calculated pressure distributions for the same case at a mid-wing station and compared with the windtunnel test results (NLR/GARTEUR calculations; ONERA S-1 test results).*

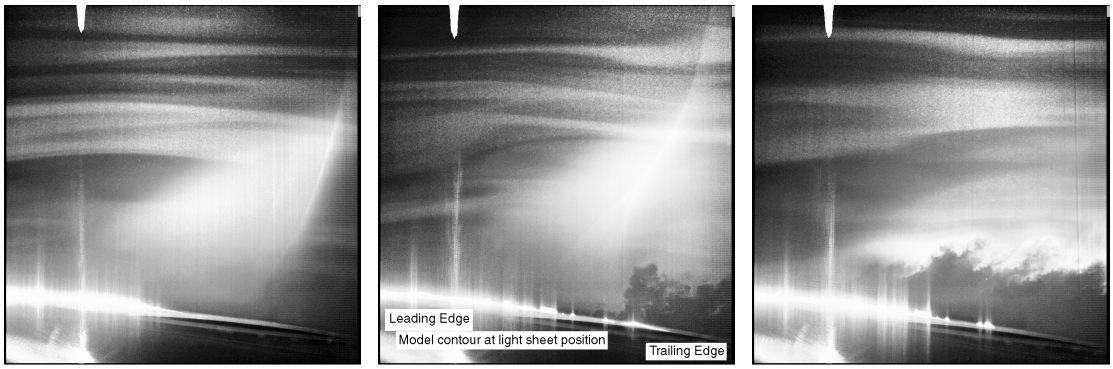


*Figure 11. Laser screen photographs of the shock wave and related separation development for an oscillating double delta wing representative of limit cycle oscillation (DNW-HST windtunnel test).*

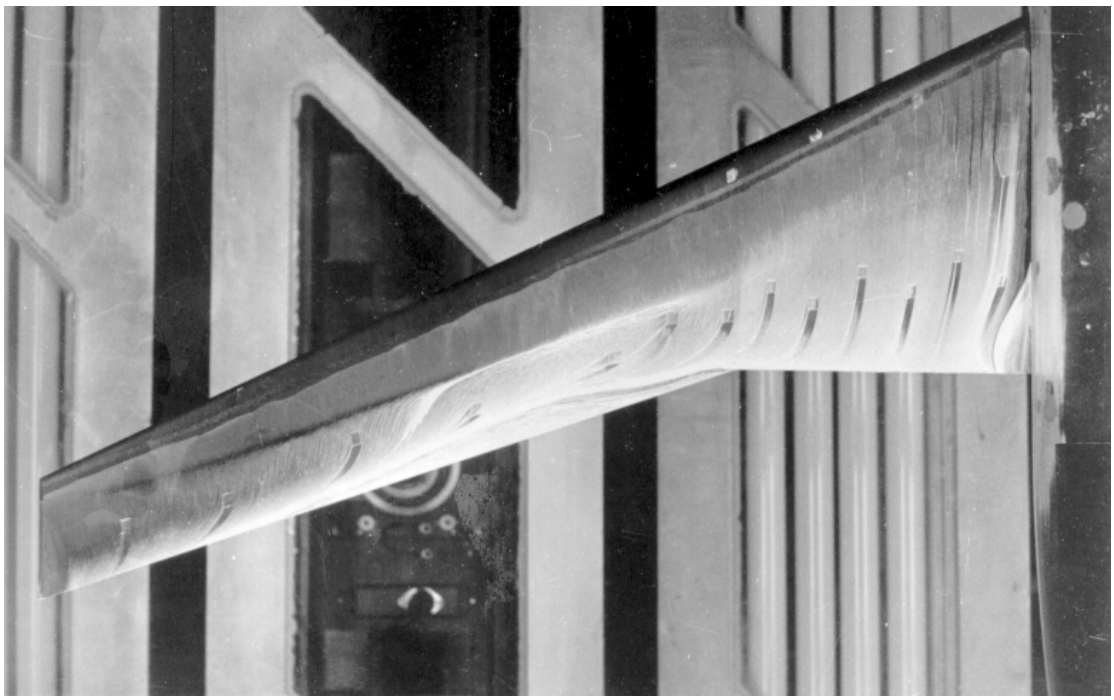

Mach=.78 $C_L$ =.6

*Figure 12. Oil flow picture of the DLR F-4 research wing indicating a shock wave and local trailing edge separation (GARTEUR; DNW-HST windtunnel tests)*

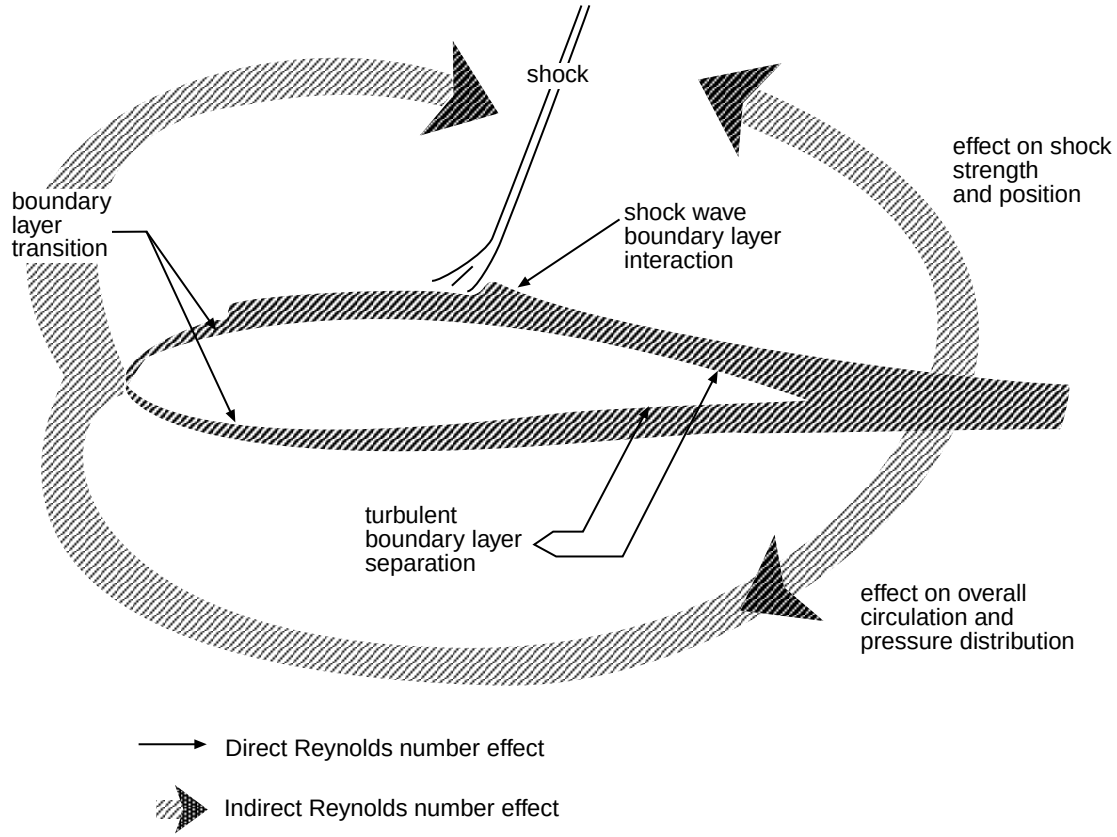


*Figure 13. Schematic representation of the transonic flow for a transport type wing illustrating the interaction between direct (viscous) and indirect (inviscid) Reynolds number effects.*

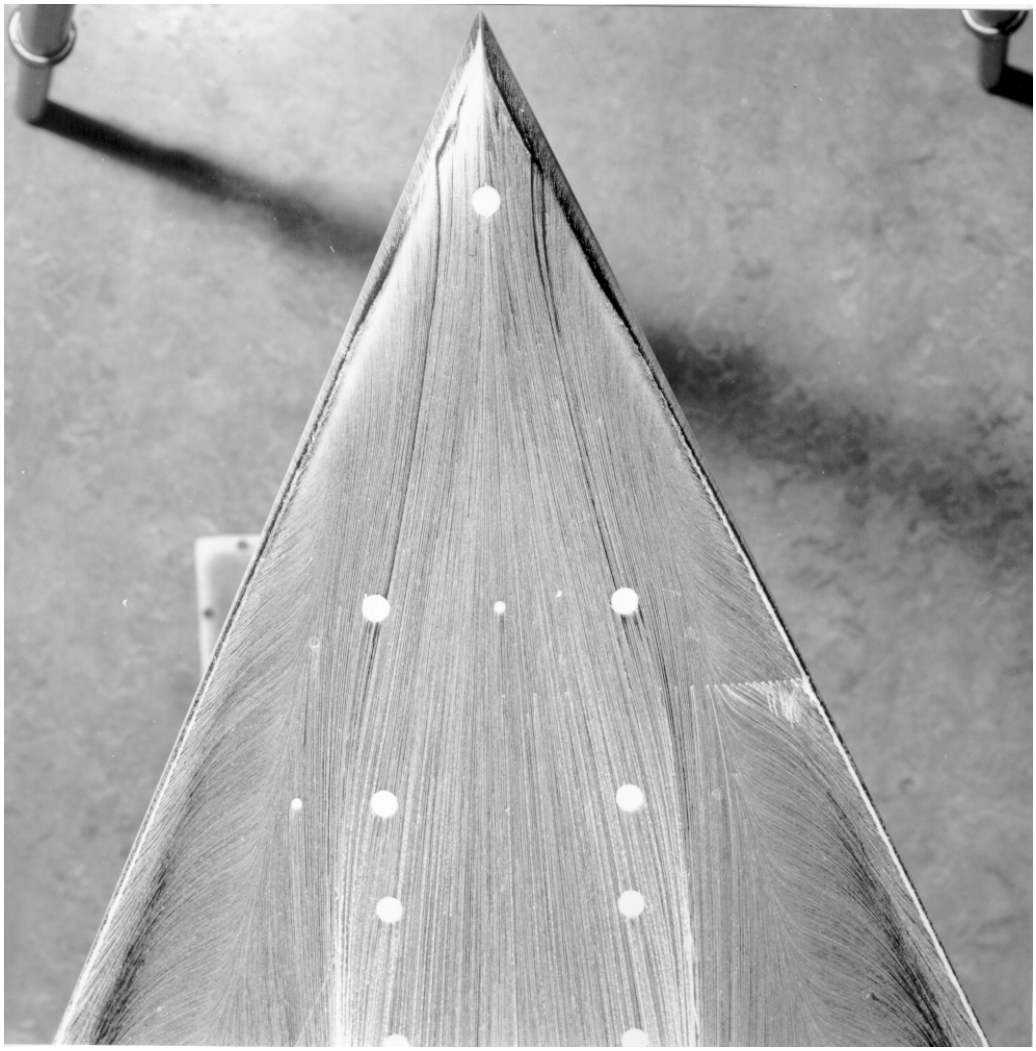

*Figure 14. Oil flow picture of the flow over a delta wing with a rounded leading edge at α=10° and Mach=.85 illustrating the formation of a primary vortex; attached flow with a laminar separation bubble near the apex develops into a primary separation at the leading edge with the corresponding attachment line more inboard (The International Vortex Flow Experiment; DNW-HST windtunnel tests).*

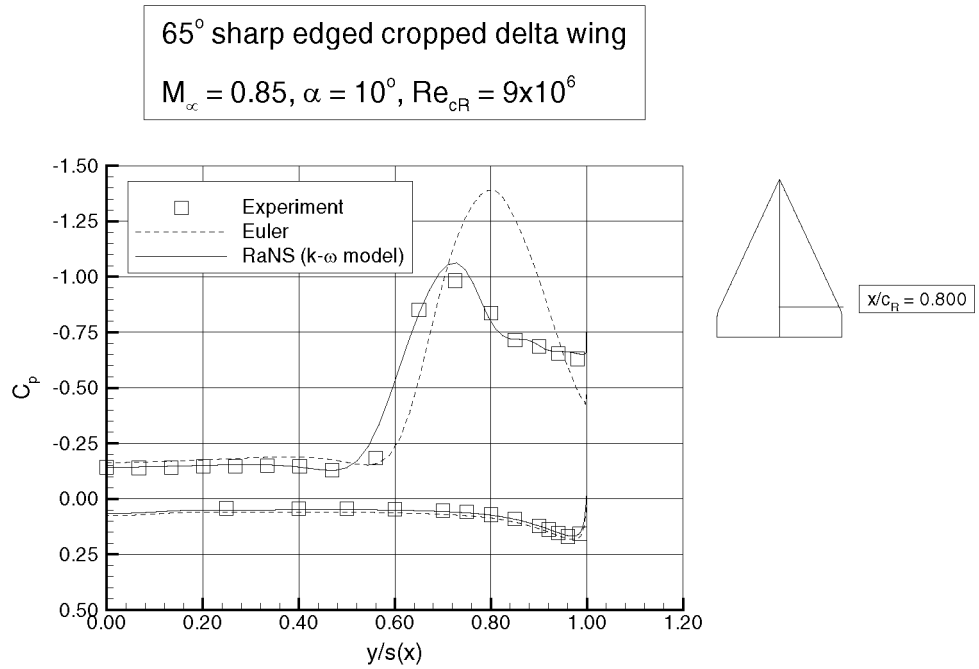


*Figure 15. Euler and Navier Stokes calculations for a sharp edged delta wing illustrating the effect of secondary (smooth) separation (NLR contribution to IEPG program).*

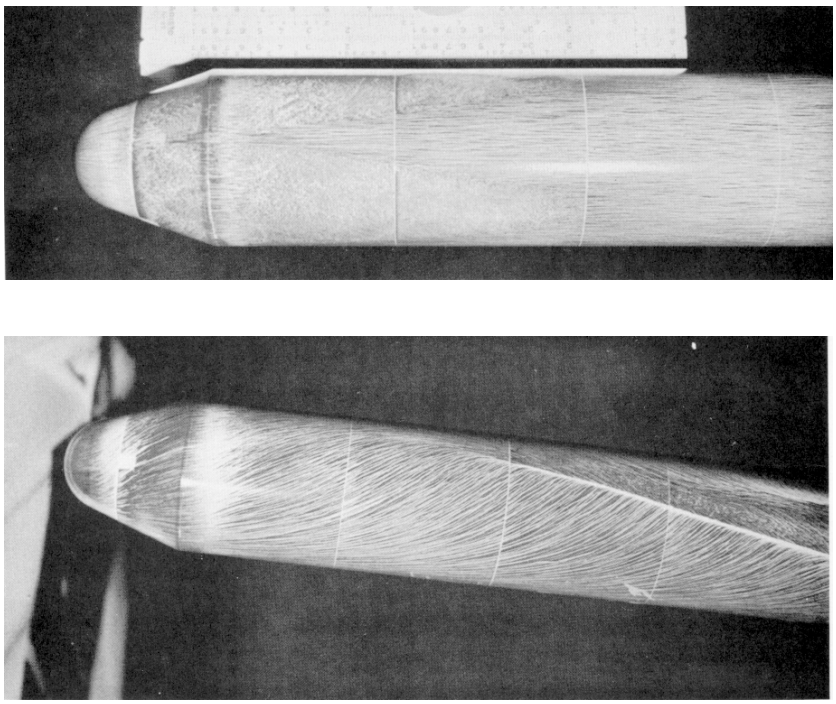

*Figure 16a. Oil flow picture of the flow over a blunted cylinder under incidence.*

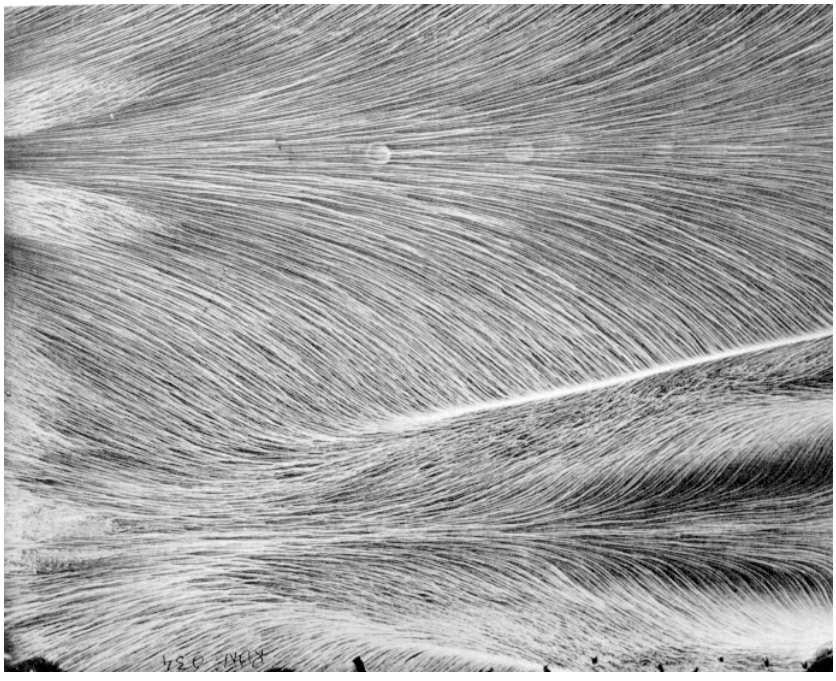

Mach=2.3

*Figure 16b. The same oil flow pattern but now on the unwrapped foil that covered the model; the primary attachment line is in the upper part of the figure; the wall streamlines run almost perpendicular into the shock (NLR experiment, DNW-CSST test results).*

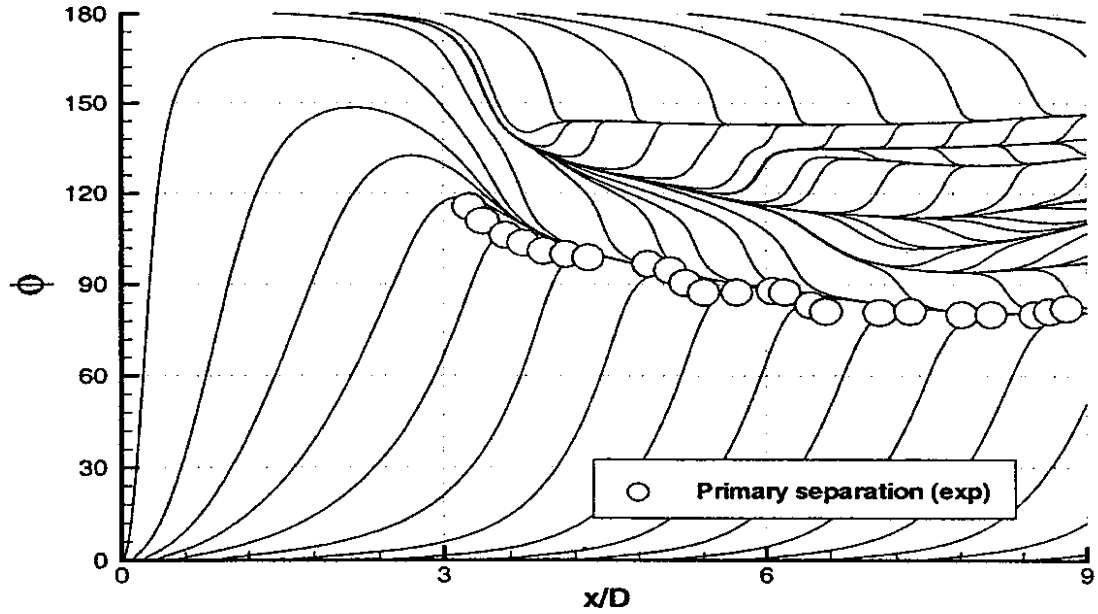


*Figure 17. Navier-Stokes calculations for an inclined cylinder with (mainly) laminar flow development; behind the primary separation secondary and even tertiary separations are visible in the calculations (calculations made by NLR for GARTEUR).*

*Figure 18. Oil flow pattern on the first supercritical wing designed by NLR showing a spiral type separation at the wing root (DNW-HST test results).*

*Figure 19. The EUROSUP model with low speed wing in the test section of the DNW-HST; the deflected leading edge is clearly visible.*

*Figure 20. Oil flow pattern of the flow for the EUROSUP model close to the low speed design condition; (a) gives an overall view and (b) a close-up of the leading edge near the kink location showing a local separation; the dark lines are indicative of vortices that are embedded in the flow.*

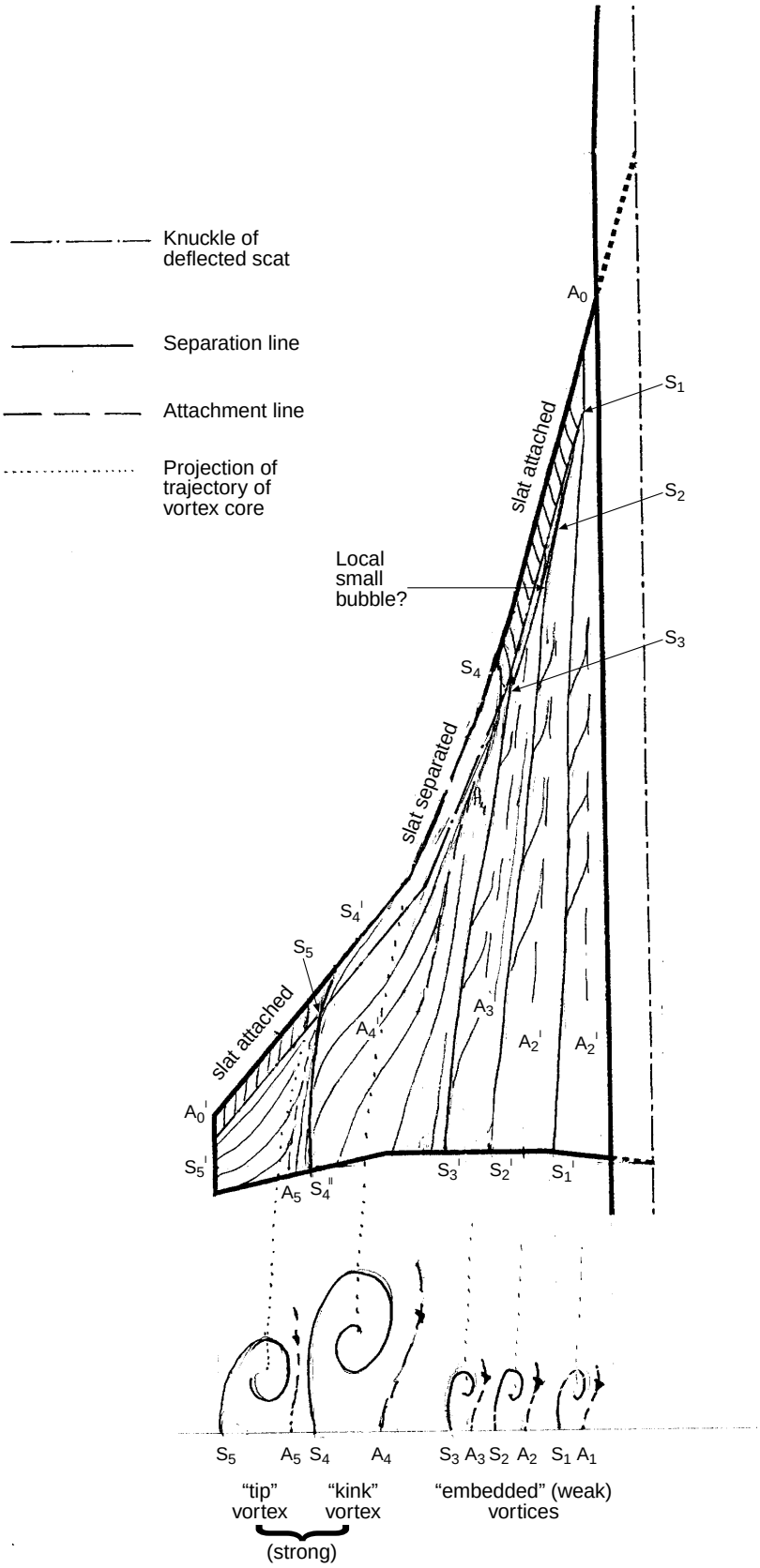


*Figure 21. Tentative interpretation of the oil flow pattern of Fig.20.*

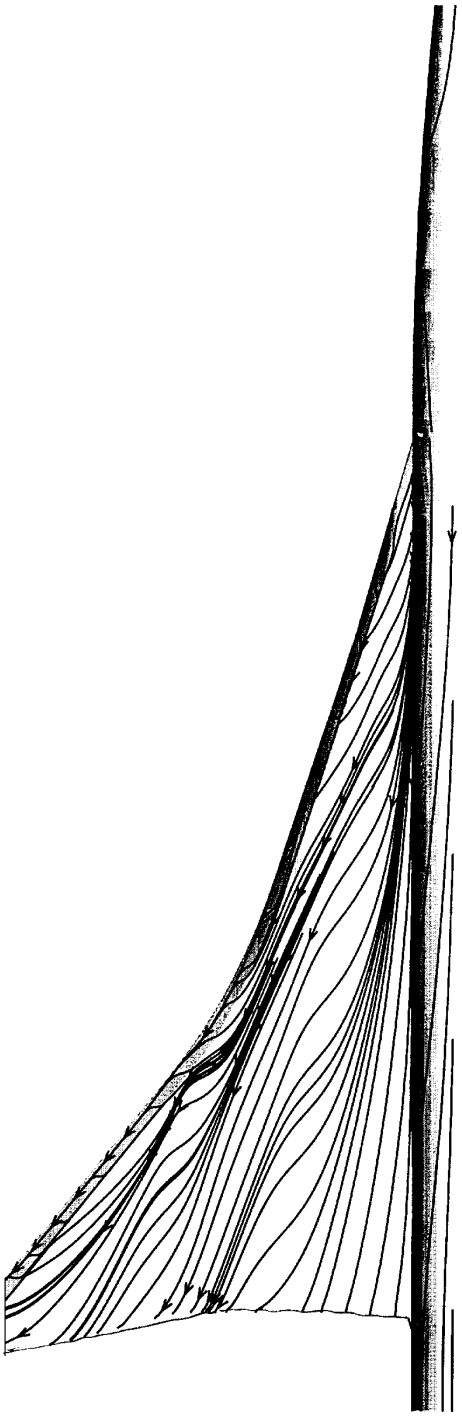

*Figure 22. Surface flow as calculated with a Navier-Stokes code showing a tendency of streamwise vortices to develop in addition to the separation in the leading edge kink region (calculations made by Van Muijden of NLR as part of a GARTEUR activity).*

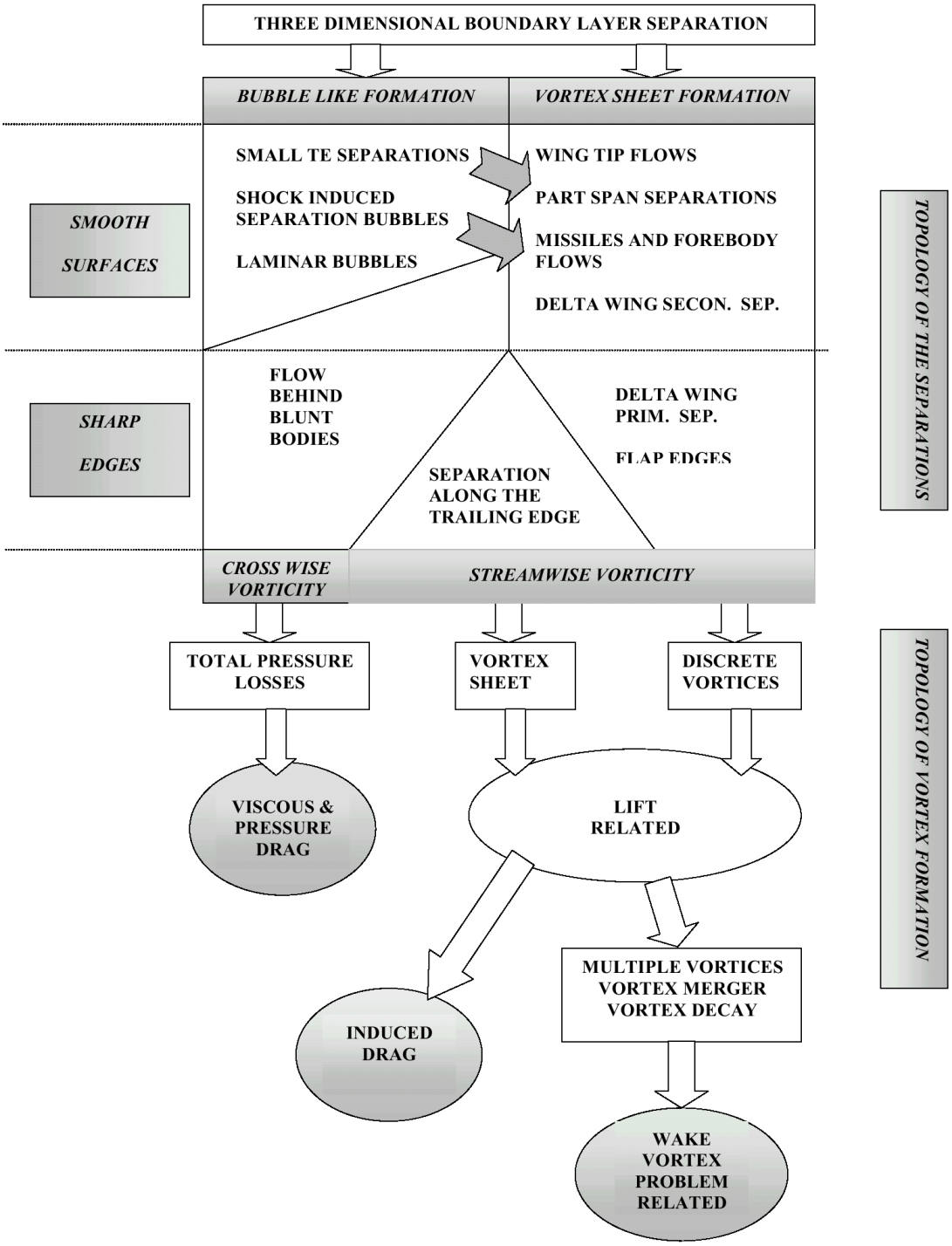


*Figure 23. Tentative scheme to relate flow separation and vortex flow development.*

*Figure 24. Flow visualization of a vortex generated by the tip of a crop-spraying aircraft.*

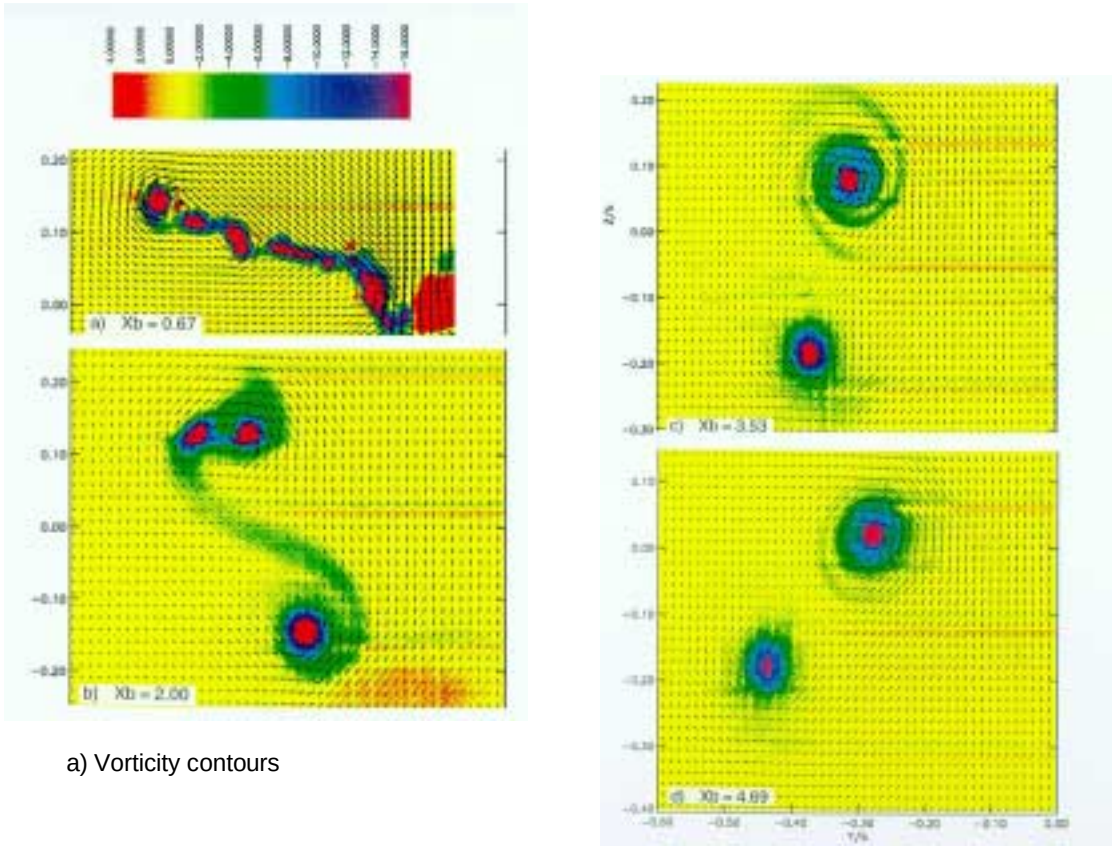


a) Vorticity contours

*Figure 25. Vorticity contours and cross-wise velocity vectors measured behind a transport type wing in landing configuration; Xb denotes the number of spans behind the aircraft (measurement made at the DNW-LST in co-operation with Boeing).*

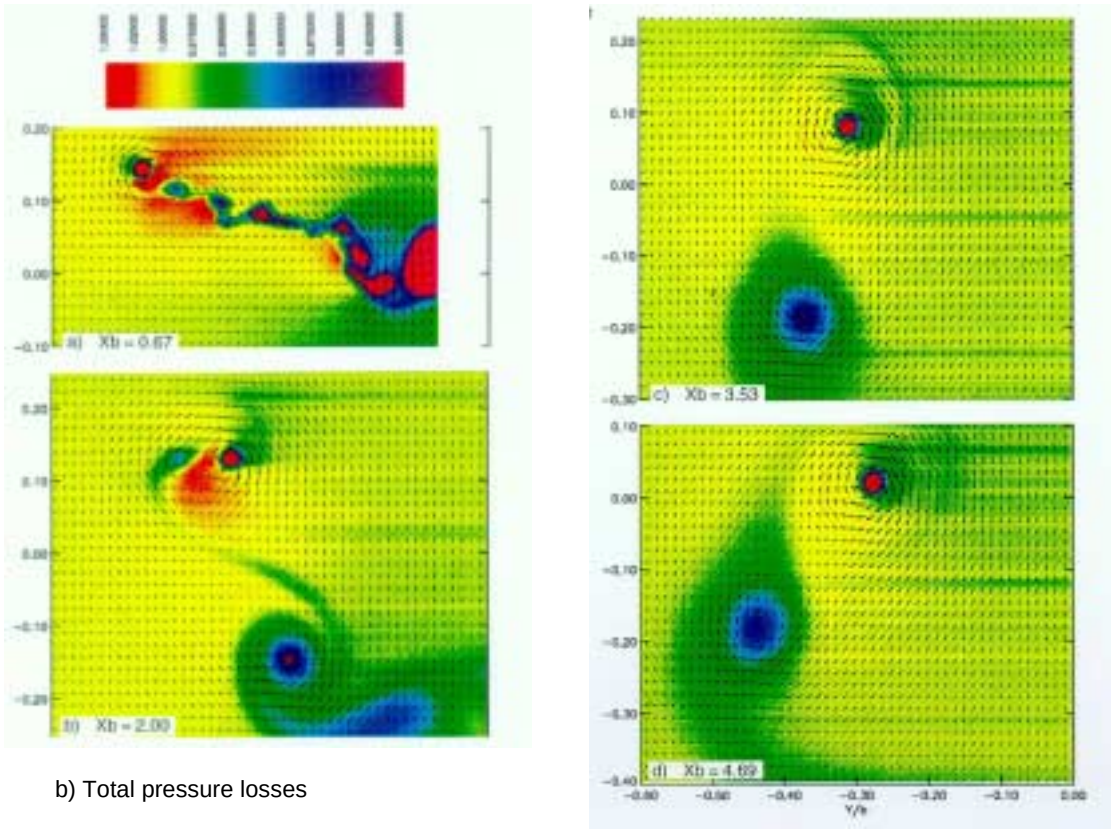


b) Total pressure losses

*Figure 26. Total pressure contours for the same stations as shown in Fig. 25; total pressure losses are entrained into the vortices.*

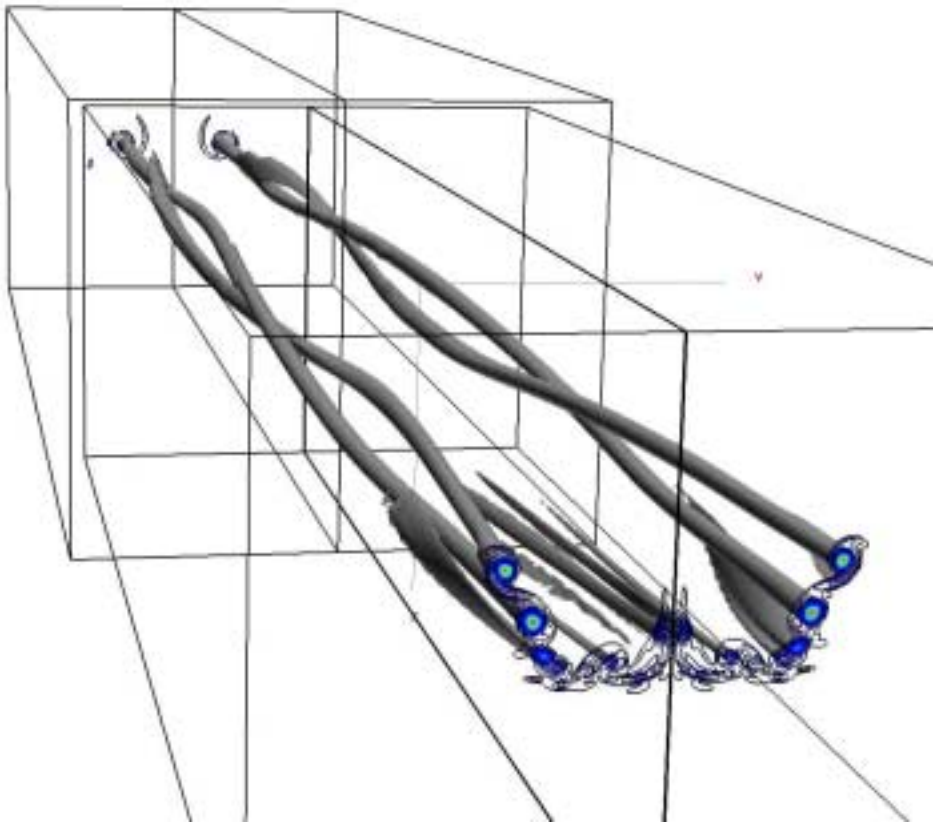

*Figure 27. Vortex roll-up and subsequent merger behind an Airbus type wing in landing configuration calculated by Laporte of CERFACS; in this case the vortex sheet rolls-up into a single pair of counter rotating vortices.*

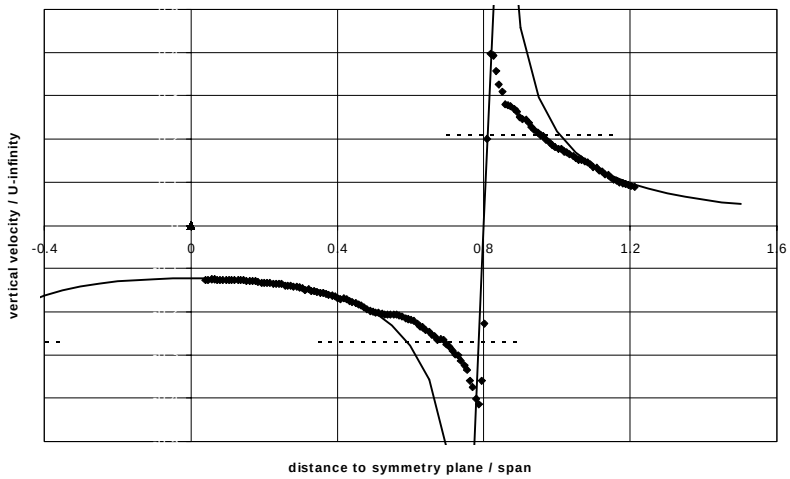


*Figure 28a. The vertical velocity induced by the vortex pair behind an Airbus type aircraft; the symbols denote the measured values in the windtunnel at 6.8 spans behind the aircraft; the solid and dotted lines follow from a simple theoretical approximation (measurements in the DNW-LFF made by Hünecke of Deutsche Airbus).*

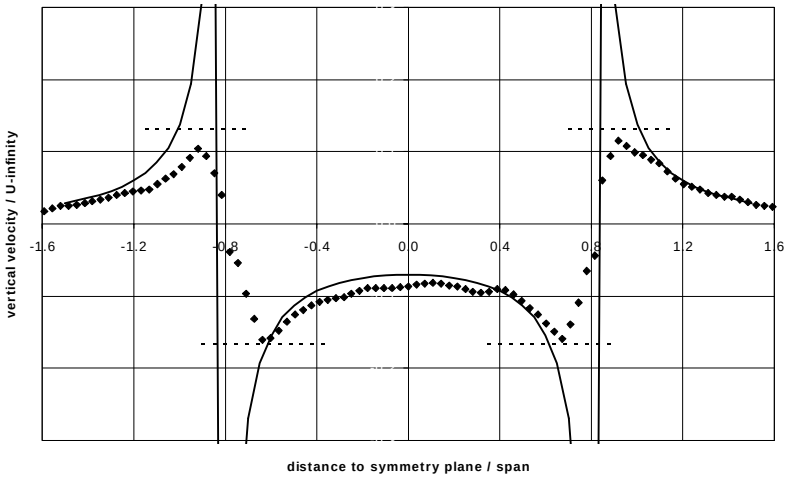


*Figure 28b. A similar picture 50 spans behind another Airbus aircraft measured at Blagnac Airport by Harris of DERA with a LIDAR system; symbols denote the measurement, the lines the simple theoretical approximation.*

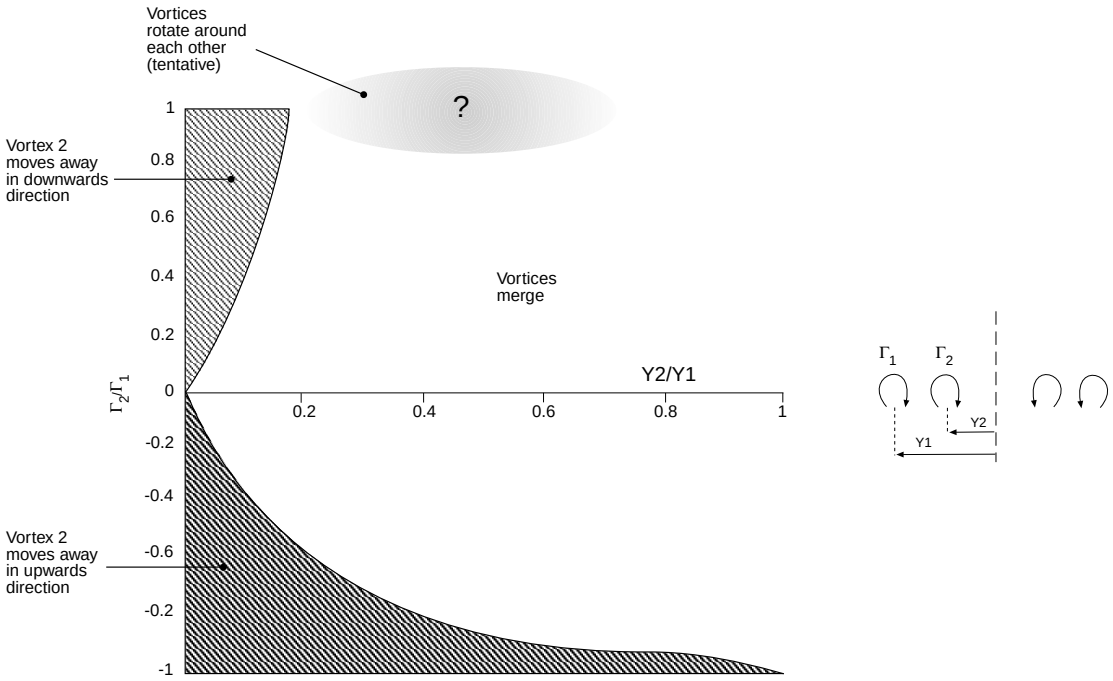


*Figure 29. Tentative representation of possible flow topologies for a double vortex pair (partly based on ref.40).*

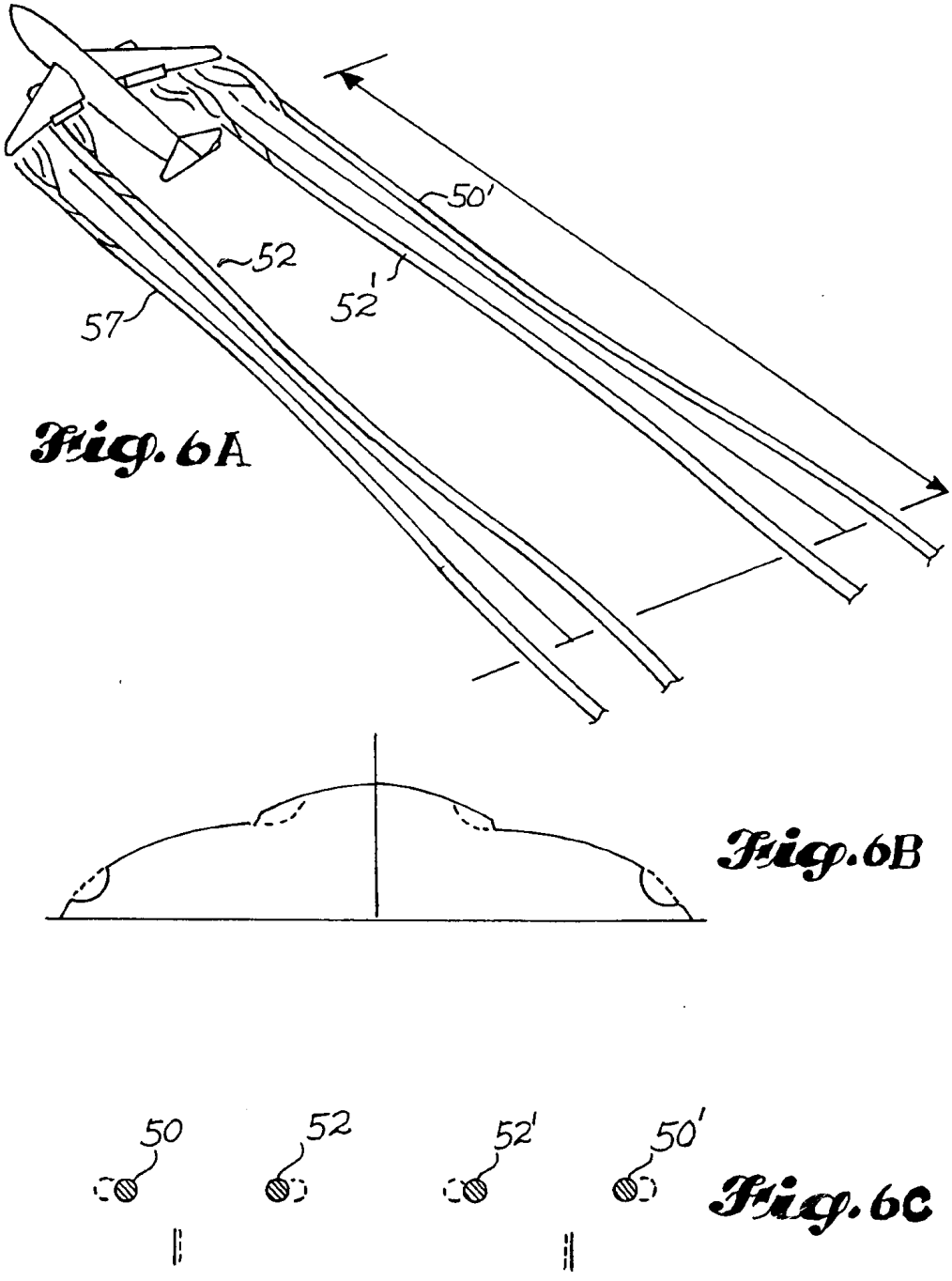


*Figure 30. Schematic representation of the vortex topology and vortex movements by excitation to enhance vortex break-down (illustration taken from the Boeing patent, ref.50).*

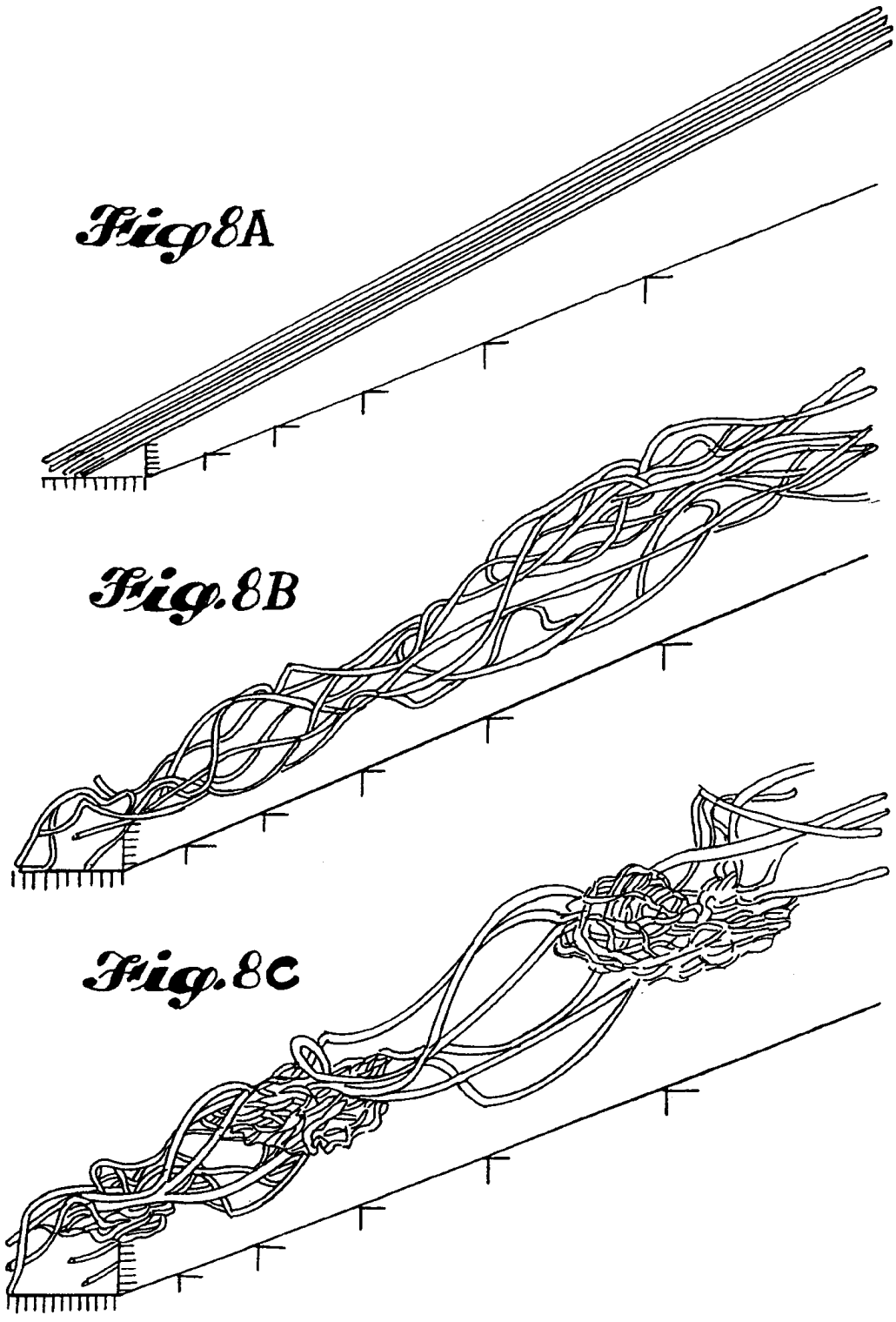


*Figure 31. Large eddy simulation illustrating the development of instabilities that cause a premature vortex breakdown (illustration taken from the Boeing patent, ref.50).*